

Paramagnetic Ions Enable Tuning of Nuclear Relaxation Rates and Provide Long-Range Structural Restraints in Solid-State NMR of Proteins

Philippe S. Nadaud, Jonathan J. Helmus, Stefanie L. Kall, and Christopher P. Jaroniec*

Department of Chemistry, The Ohio State University, Columbus, Ohio 43210

Received January 12, 2009; E-mail: jaroniec@chemistry.ohio-state.edu

Abstract: Magic-angle-spinning solid-state nuclear magnetic resonance (SSNMR) studies of natively diamagnetic uniformly ^{13}C , ^{15}N -enriched proteins, intentionally modified with side chains containing paramagnetic ions, are presented, with the aim of using the concomitant nuclear paramagnetic relaxation enhancements (PREs) as a source of long-range structural information. The paramagnetic ions are incorporated at selected sites in the protein as EDTA–metal complexes by introducing a solvent-exposed cysteine residue using site-directed mutagenesis, followed by modification with a thiol-specific reagent, *N*-(*S*-(2-pyridylthio)cysteaminyl)EDTA-metal. Here, this approach is demonstrated for the K28C and T53C mutants of B1 immunoglobulin-binding domain of protein G (GB1), modified with EDTA-Mn $^{2+}$ and EDTA-Cu $^{2+}$ side chains. It is shown that incorporation of paramagnetic moieties, exhibiting different relaxation times and spin quantum numbers, facilitates the convenient modulation of longitudinal (R_1) and transverse (R_2 , $R_{1\rho}$) relaxation rates of the protein ^1H , ^{13}C , and ^{15}N nuclei. Specifically, the EDTA-Mn $^{2+}$ side chain generates large distance-dependent transverse relaxation enhancements, analogous to those observed previously in the presence of nitroxide spin labels, while this phenomenon is significantly attenuated for the Cu $^{2+}$ center. Both Mn $^{2+}$ and Cu $^{2+}$ ions cause considerable longitudinal nuclear PREs. The combination of negligible transverse and substantial longitudinal relaxation enhancements obtained with the EDTA-Cu $^{2+}$ side chain is especially advantageous, because it enables structural restraints for most sites in the protein to be readily accessed via quantitative, site-resolved measurements of nuclear R_1 rate constants by multidimensional SSNMR methods. This is demonstrated here for backbone amide ^{15}N nuclei, using methods based on 2D ^{15}N – ^{13}C chemical shift correlation spectroscopy. The measured longitudinal PREs are found to be highly correlated with the proximity of the Cu $^{2+}$ ion to ^{15}N spins, with significant effects observed for nuclei up to ~ 20 Å away, thereby providing important information about protein structure on length scales that are inaccessible to traditional SSNMR techniques.

Introduction

Magic-angle spinning (MAS) solid-state nuclear magnetic resonance (SSNMR) is rapidly emerging as a unique spectroscopic tool, with immense potential for providing atomic-resolution images of biomacromolecules that cannot be readily analyzed by traditional high-resolution techniques.^{1–4} At the present time, complete or nearly complete backbone and side-chain ^{13}C and ^{15}N resonance assignments can be established for uniformly ^{13}C , ^{15}N -enriched proteins up to ~ 100 amino acid residues^{5–18} by using a variety of two- and three-dimensional SSNMR chemical shift correlation schemes.^{19,20} This provides

the basis for the acquisition of additional multidimensional SSNMR spectra that report on the magnitudes and relative orientations of internuclear dipolar coupling tensors, and thus

- (1) McDermott, A. E. *Curr. Opin. Struct. Biol.* **2004**, *14*, 554–561.
- (2) Hughes, C. E.; Baldus, M. *Annu. Rep. NMR Spectrosc.* **2005**, *55*, 121–158.
- (3) Tycko, R. *Q. Rev. Biophys.* **2006**, *39*, 1–55.
- (4) Bockmann, A. *Angew. Chem., Int. Ed.* **2008**, *47*, 6110–6113.
- (5) McDermott, A.; Polenova, T.; Bockmann, A.; Zilm, K. W.; Paulsen, E. K.; Martin, R. W.; Montelione, G. T. *J. Biomol. NMR* **2000**, *16*, 209–219.
- (6) Pauli, J.; Baldus, M.; van Rossum, B.; de Groot, H.; Oschkinat, H. *Chembiochem* **2001**, *2*, 272–281.
- (7) Bockmann, A.; Lange, A.; Galinier, A.; Luca, S.; Giraud, N.; Juy, M.; Heise, H.; Monserret, R.; Penin, F.; Baldus, M. *J. Biomol. NMR* **2003**, *27*, 323–339.
- (8) Igumenova, T. I.; McDermott, A. E.; Zilm, K. W.; Martin, R. W.; Paulson, E. K.; Wand, A. J. *J. Am. Chem. Soc.* **2004**, *126*, 6720–6727.
- (9) van Gammeren, A. J.; Hulsbergen, F. B.; Hollander, J. G.; de Groot, H. J. M. *J. Biomol. NMR* **2005**, *31*, 279–293.
- (10) Marulanda, D.; Tasayco, M. L.; Cataldi, M.; Arriaran, V.; Polenova, T. *J. Phys. Chem. B* **2005**, *109*, 18135–18145.
- (11) Franks, W. T.; Zhou, D. H.; Wylie, B. J.; Money, B. G.; Graesser, D. T.; Frericks, H. L.; Sahota, G.; Rienstra, C. M. *J. Am. Chem. Soc.* **2005**, *127*, 12291–12305.
- (12) Heise, H.; Hoyer, W.; Becker, S.; Andronesi, O. C.; Riedel, D.; Baldus, M. *Proc. Natl. Acad. Sci. U.S.A.* **2005**, *102*, 15871–15876.
- (13) Siemer, A. B.; Ritter, C.; Steinmetz, M. O.; Ernst, M.; Riek, R.; Meier, B. H. *J. Biomol. NMR* **2006**, *34*, 75–87.
- (14) Goldbourt, A.; Gross, B. J.; Day, L. A.; McDermott, A. E. *J. Am. Chem. Soc.* **2007**, *129*, 2338–2344.
- (15) Pintacuda, G.; Giraud, N.; Pierattelli, R.; Bockmann, A.; Bertini, I.; Emsley, L. *Angew. Chem., Int. Ed.* **2007**, *46*, 1079–1082.

yield distance^{21–34} and dihedral angle^{35–43} restraints. Altogether, the ability to collect multiple site-specific structural restraints of this type has led to the de novo determination of relatively high-resolution, three-dimensional SSNMR structures for several peptides and proteins.^{26,44–52}

In spite of these exciting recent developments, the determination of high-quality atomic-resolution protein structures by SSNMR is still far from routine and continues to pose significant challenges. One of the foremost difficulties is related to the relative paucity of unambiguous long-range distance restraints—which serve as the primary source of information about the overall protein fold—that can be obtained by using the existing SSNMR methods. This stems from the fact that, as noted above, such distance restraints are invariably derived from through-space magnetic dipole–dipole couplings⁵³ between the protein ¹H, ¹³C, and ¹⁵N nuclei ($D \propto \gamma_I \gamma_S / r^3$, where γ_I and γ_S are the gyromagnetic ratios of nuclear spins I and S, and r is the internuclear distance), which become difficult to detect and/or quantify within extensively coupled multispin networks for distances significantly in excess of $\sim 5\text{--}6$ Å. One general approach that can potentially alleviate this problem and yield a multitude of long-range, up to $\sim 20\text{--}25$ Å, structural restraints in uniformly ¹³C, ¹⁵N-enriched proteins involves multidimensional SSNMR studies of protein molecules intentionally modified with covalently attached paramagnetic tags; the underlying principle behind this approach is the fact that the electron gyromagnetic ratio, γ_e , is $\sim 2\text{--}3$ orders of magnitude larger than nuclear gyromagnetic ratios, γ_n (e.g., for protons⁵⁴ $|\gamma_e/\gamma_n| \approx 658$), resulting in considerable electron–nucleus dipolar interactions even at large distances.

As thoroughly discussed elsewhere,^{53,55} the introduction of an arbitrary paramagnetic center into the molecule of interest can elicit major electron–nucleus distance-dependent NMR spectral changes that include Fermi contact and dipolar or pseudocontact shifts ($\delta^{pc} \propto r^{-3}$, where r is the electron–nucleus distance) of the resonance frequencies. Moreover, the fluctuating magnetic fields generated at the sites of the nuclei by electron spin relaxation and/or molecular dynamics lead to enhanced longitudinal (R_1) and transverse ($R_2, R_{1\rho}$) nuclear spin relaxation rates,^{55–58} where the dipolar contribution to these paramagnetic

- (16) Nadaud, P. S.; Helmus, J. J.; Jaroniec, C. P. *Biomol. NMR Assign.* **2007**, *1*, 117–120.
- (17) Helmus, J. J.; Surewicz, K.; Nadaud, P. S.; Surewicz, W. K.; Jaroniec, C. P. *Proc. Natl. Acad. Sci. U.S.A.* **2008**, *105*, 6284–6289.
- (18) Li, Y.; Berthold, D. A.; Gennis, R. B.; Rienstra, C. M. *Protein Sci.* **2008**, *17*, 199–204.
- (19) Baldus, M. *Prog. NMR Spectrosc.* **2002**, *41*, 1–47.
- (20) Straus, S. K. *Philos. Trans. R. Soc. London B* **2004**, *359*, 997–1008.
- (21) Lange, A.; Luca, S.; Baldus, M. *J. Am. Chem. Soc.* **2002**, *124*, 9704–9705.
- (22) Reif, B.; van Rossum, B. J.; Castellani, F.; Rehbein, K.; Diehl, A.; Oschkinat, H. *J. Am. Chem. Soc.* **2003**, *125*, 1488–1489.
- (23) Paulson, E. K.; Morcombe, C. R.; Gaponenko, V.; Dancheck, B.; Byrd, R. A.; Zilm, K. W. *J. Am. Chem. Soc.* **2003**, *125*, 14222–14223.
- (24) Zhou, D. H.; Shah, G.; Cormos, M.; Mullen, C.; Sandoz, D.; Rienstra, C. M. *J. Am. Chem. Soc.* **2007**, *129*, 11791–11801.
- (25) Takegoshi, K.; Nomura, K.; Terao, T. *Chem. Phys. Lett.* **1995**, *232*, 424–428.
- (26) Castellani, F.; van Rossum, B.; Diehl, A.; Schubert, M.; Rehbein, K.; Oschkinat, H. *Nature* **2002**, *420*, 98–102.
- (27) Ladizhansky, V.; Griffin, R. G. *J. Am. Chem. Soc.* **2004**, *126*, 948–958.
- (28) Paravastu, A. K.; Tycko, R. *J. Chem. Phys.* **2006**, *124*, 194303.
- (29) Peng, X.; Libich, D.; Janik, R.; Harauz, G.; Ladizhansky, V. *J. Am. Chem. Soc.* **2008**, *130*, 359–369.
- (30) Jaroniec, C. P.; Tounge, B. A.; Herzfeld, J.; Griffin, R. G. *J. Am. Chem. Soc.* **2001**, *123*, 3507–3519.

relaxation enhancements (PREs, also denoted here as Γ_1 , Γ_2 , and $\Gamma_{1\rho}$) is a particularly valuable source of structural information. According to the Solomon relaxation mechanism, the nuclear PREs due to the dipolar coupling with unpaired electrons can be expressed as^{55–58}

$$\Gamma_1 \approx \frac{2}{15} \left(\frac{\mu_0}{4\pi} \right)^2 \gamma_n^2 g_e^2 \mu_B^2 S(S+1) \left(\frac{3\tau_{c1}}{1 + \omega_n^2 \tau_{c1}^2} + \frac{7\tau_{c2}}{1 + \omega_e^2 \tau_{c2}^2} \right) \quad (1)$$

$$\Gamma_2 \approx \Gamma_{1\rho} \approx \frac{1}{15} \left(\frac{\mu_0}{4\pi} \right)^2 \gamma_n^2 g_e^2 \mu_B^2 S(S+1) \left(4\tau_{c1} + \frac{3\tau_{c1}}{1 + \omega_n^2 \tau_{c1}^2} + \frac{13\tau_{c2}}{1 + \omega_e^2 \tau_{c2}^2} \right) \quad (2)$$

where μ_0 is the permeability of free space, γ_n is the nuclear gyromagnetic ratio, g_e is the electron *g*-value, μ_B is the Bohr

- (31) Jaroniec, C. P.; Lansing, J. C.; Tounge, B. A.; Belenky, M.; Herzfeld, J.; Griffin, R. G. *J. Am. Chem. Soc.* **2001**, *123*, 12929–12930.
- (32) Jaroniec, C. P.; Filip, C.; Griffin, R. G. *J. Am. Chem. Soc.* **2002**, *124*, 10728–10742.
- (33) Lewandowski, J. R.; De Paepe, G.; Griffin, R. G. *J. Am. Chem. Soc.* **2007**, *129*, 728–729.
- (34) Helmus, J. J.; Nadaud, P. S.; Hofer, N.; Jaroniec, C. P. *J. Chem. Phys.* **2008**, *128*, 052314.
- (35) Feng, X.; Lee, Y. K.; Sandström, D.; Eden, M.; Maisel, H.; Sebald, A.; Levitt, M. H. *Chem. Phys. Lett.* **1996**, *257*, 314–320.
- (36) Ishii, Y.; Terao, T.; Kainosh, M. *Chem. Phys. Lett.* **1996**, *256*, 133–140.
- (37) Hong, M.; Gross, J. D.; Griffin, R. G. *J. Phys. Chem. B* **1997**, *101*, 5869–5874.
- (38) Costa, P. R.; Gross, J. D.; Hong, M.; Griffin, R. G. *Chem. Phys. Lett.* **1997**, *280*, 95–103.
- (39) Feng, X.; Eden, M.; Brinkmann, A.; Luthman, H.; Eriksson, L.; Gräslund, A.; Antzutkin, O. N.; Levitt, M. H. *J. Am. Chem. Soc.* **1997**, *119*, 12006–12007.
- (40) Reif, B.; Hohwy, M.; Jaroniec, C. P.; Rienstra, C. M.; Griffin, R. G. *J. Magn. Reson.* **2000**, *145*, 132–141.
- (41) Ladizhansky, V.; Veshtort, M.; Griffin, R. G. *J. Magn. Reson.* **2002**, *154*, 317–324.
- (42) Rienstra, C. M.; Hohwy, M.; Mueller, L. J.; Jaroniec, C. P.; Reif, B.; Griffin, R. G. *J. Am. Chem. Soc.* **2002**, *124*, 11908–11922.
- (43) Ladizhansky, V.; Jaroniec, C. P.; Diehl, A.; Oschkinat, H.; Griffin, R. G. *J. Am. Chem. Soc.* **2003**, *125*, 6827–6833.
- (44) Rienstra, C. M.; Tucker-Kellogg, L.; Jaroniec, C. P.; Hohwy, M.; Reif, B.; Lozano-Perez, T.; Tidor, B.; Griffin, R. G. *Proc. Natl. Acad. Sci. U.S.A.* **2002**, *99*, 10260–10265.
- (45) Jaroniec, C. P.; MacPhee, C. E.; Bajaj, V. S.; McMahon, M. T.; Dobson, C. M.; Griffin, R. G. *Proc. Natl. Acad. Sci. U.S.A.* **2004**, *101*, 711–716.
- (46) Zech, S. G.; Wand, A. J.; McDermott, A. E. *J. Am. Chem. Soc.* **2005**, *127*, 8618–8626.
- (47) Iwata, K.; Fujiwara, T.; Matsuki, Y.; Akutsu, H.; Takahashi, S.; Naiki, H.; Goto, Y. *Proc. Natl. Acad. Sci. U.S.A.* **2006**, *103*, 18119–18124.
- (48) Zhou, D. H.; Shea, J. J.; Nieuwkoop, A. J.; Franks, W. T.; Wylie, B. J.; Mullen, C.; Sandoz, D.; Rienstra, C. M. *Angew. Chem., Int. Ed.* **2007**, *46*, 8380–8383.
- (49) Manolikas, T.; Herrmann, T.; Meier, B. H. *J. Am. Chem. Soc.* **2008**, *130*, 3959–3966.
- (50) Korukottu, J.; Schneider, R.; Vijayan, V.; Lange, A.; Pongs, O.; Becker, S.; Baldus, M.; Zweckstetter, M. *PLoS ONE* **2008**, *3*, e2359.
- (51) Loquet, A.; Bardiaux, B.; Gardiennet, C.; Blanchet, C.; Baldus, M.; Nilges, M.; Malliaiv, T.; Bockmann, A. *J. Am. Chem. Soc.* **2008**, *130*, 3579–3589.
- (52) Wasmer, C.; Lange, A.; Van Melckebeke, H.; Siemer, A. B.; Riek, R.; Meier, B. H. *Science* **2008**, *319*, 1523–1526.
- (53) Abragam, A. *Principles of Nuclear Magnetism*; Oxford University Press: New York, 1961.
- (54) Koenig, S. H.; Prodell, A. G.; Kusch, P. *Phys. Rev.* **1952**, *88*, 191–199.
- (55) Bertini, I.; Luchinat, C.; Parigi, G. *Solution NMR of Paramagnetic Molecules: Applications to Metallobiomolecules and Models*; Elsevier: Amsterdam, 2001.

magneton, S is the electron spin quantum number, r is the electron–nucleus distance, and ω_n and ω_e are the Larmor frequencies of the nucleus and electron, respectively. In general, the correlation times, τ_{c1} and τ_{c2} , contain contributions from longitudinal and transverse electron spin relaxation (characterized by time constants T_{1e} and T_{2e} , respectively), molecular tumbling (rotational correlation time, τ_r) and chemical exchange (exchange correlation time, τ_M), and are given by

$$\frac{1}{\tau_{c1}} = \frac{1}{T_{1e}} + \frac{1}{\tau_r} + \frac{1}{\tau_M} \quad (3)$$

$$\frac{1}{\tau_{c2}} = \frac{1}{T_{2e}} + \frac{1}{\tau_r} + \frac{1}{\tau_M} \quad (4)$$

Note, however, that a single electronic relaxation time, $T_{1e} = T_{2e}$, can often be assumed to a reasonable approximation. Furthermore, in the solid phase the τ_r and τ_M terms can typically be neglected—i.e., for solids, a single electron correlation time, $\tau_{c1} = \tau_{c2} = T_{1e}$, may be used in eqs 1 and 2. In summary, albeit the precise effects on the NMR spectrum induced by the presence of a paramagnetic moiety depend on multiple factors including the physical state of the sample as well as different electronic and molecular parameters, several generalizations can be made. First, contact shifts are expected to be negligible for nuclei that are significantly removed from the paramagnetic center. Second, paramagnetic species characterized by small electron g -tensor anisotropies and T_{1e} values in the nanosecond–microsecond regime (e.g., Mn^{2+} and Cu^{2+} ions, and nitroxide spin labels) are expected to generate small pseudocontact shifts and relatively large transverse nuclear PREs, while those with larger g -anisotropies and subpicosecond T_{1e} 's (e.g., lanthanide ions except Gd^{3+}) tend to yield considerable δ^{pc} and negligible transverse PREs.⁵⁵

NMR measurements of nuclear PREs and pseudocontact shifts for biological macromolecules in solution have a long and rich history, highlighted by numerous applications to the analysis of enzyme active sites, protein and nucleic acid structure, and intermolecular interactions.^{55,59–63} In comparison, the vast majority of NMR studies of paramagnetic biological solids, published during the past several decades, have focused on small metal coordination complexes,^{64–78} with only a handful of landmark applications to peptides and proteins aimed at the

characterization of local structure at specific sites,^{79–87} determination of the mode of membrane insertion,^{88,89} or the modulation of 1H longitudinal relaxation for spectral sensitivity enhancement.^{90–92} More recently, however, several multidimensional MAS NMR studies of uniformly ^{13}C , ^{15}N -labeled paramagnetic proteins in the microcrystalline solid phase have been reported, including ^{13}C and ^{15}N resonance assignments of human copper(II)–zinc(II) superoxide dismutase,¹⁵ measurements of ^{13}C pseudocontact shifts in cobalt(II)-substituted catalytic domain of matrix metalloproteinase 12,^{93,94} and observation of site-resolved long-range nuclear PRE effects in nitroxide spin-labeled analogues of the B1 immunoglobulin binding domain of protein G (GB1).⁹⁵ These studies clearly demonstrate that not only are multidimensional SSNMR experiments on ^{13}C , ^{15}N -enriched paramagnetic proteins generally feasible, but that, in fact, such experiments have the capacity to provide novel types of site-specific structural data for biological macromolecules on length scales that are inaccessible to traditional SSNMR methods.

In our recent study of spin-labeled GB1 variants, we have shown that multiple site-specific structural restraints could be simultaneously obtained for protein nuclei located up to ~ 20 Å from the radical.⁹⁵ These restraints were derived by monitor-

- (56) Solomon, I. *Phys. Rev.* **1955**, *99*, 559–565.
- (57) Bloembergen, N.; Morgan, L. O. *J. Chem. Phys.* **1961**, *34*, 842–850.
- (58) Koenig, S. H. *J. Magn. Reson.* **1982**, *47*, 441–453.
- (59) Krugh, T. R. In *Spin Labeling: Theory and Applications*; Academic Press: New York, 1976.
- (60) Kosen, P. A. *Methods Enzymol.* **1989**, *177*, 86–121.
- (61) Arnesano, F.; Banci, L.; Piccioli, M. *Q. Rev. Biophys.* **2005**, *38*, 167–219.
- (62) Clore, G. M.; Tang, C.; Iwahara, J. *Curr. Opin. Struct. Biol.* **2007**, *17*, 603–616.
- (63) Pintacuda, G.; John, M.; Su, X. C.; Otting, G. *Acc. Chem. Res.* **2007**, *40*, 206–212.
- (64) Ganapathy, S.; Naito, A.; McDowell, C. A. *J. Am. Chem. Soc.* **1981**, *103*, 6011–6015.
- (65) Chacko, V. P.; Ganapathy, S.; Bryant, R. G. *J. Am. Chem. Soc.* **1983**, *105*, 5491–5492.
- (66) Walter, T. H.; Oldfield, E. *J. Chem. Soc., Chem. Commun.* **1987**, 646–647.
- (67) Nayee, A.; Yesinowski, J. P. *J. Chem. Phys.* **1988**, *89*, 4600–4608.
- (68) Campbell, G. C.; Haw, J. F. *Inorg. Chem.* **1988**, *27*, 3706–3709.
- (69) Groombridge, C. J.; Perkins, M. J. *J. Chem. Soc., Chem. Commun.* **1991**, 1164–1166.
- (70) Brough, A. R.; Grey, C. P.; Dobson, C. M. *J. Am. Chem. Soc.* **1993**, *115*, 7318–7327.
- (71) Liu, K.; Ryan, D.; Nakanishi, K.; McDermott, A. E. *J. Am. Chem. Soc.* **1995**, *117*, 6897–6906.
- (72) Lee, H.; Polenova, T.; Beer, R. H.; McDermott, A. E. *J. Am. Chem. Soc.* **1999**, *121*, 6884–6894.
- (73) Heise, H.; Kohler, F. H.; Mota, F.; Novoa, J. J.; Veciana, J. *J. Am. Chem. Soc.* **1999**, *121*, 9659–9667.
- (74) Zhang, Y.; Sun, H. H.; Oldfield, E. *J. Am. Chem. Soc.* **2005**, *127*, 3652–3653.
- (75) Ishii, Y.; Wickramasinghe, N. P.; Chimon, S. *J. Am. Chem. Soc.* **2003**, *125*, 3438–3439.
- (76) Wickramasinghe, N. P.; Shaibat, M.; Ishii, Y. *J. Am. Chem. Soc.* **2005**, *127*, 5796–5797.
- (77) Wickramasinghe, N. P.; Ishii, Y. *J. Magn. Reson.* **2006**, *181*, 233–243.
- (78) Wickramasinghe, N. P.; Shaibat, M. A.; Jones, C. R.; Casabianca, L. B.; de Dios, A. C.; Harwood, J. S.; Ishii, Y. *J. Chem. Phys.* **2008**, *128*, 052210.
- (79) Rothgeb, T. M.; Oldfield, E. *J. Biol. Chem.* **1981**, *256*, 1432–1446.
- (80) Lee, R. W.; Oldfield, E. *J. Biol. Chem.* **1982**, *257*, 5023–5029.
- (81) Zysmilich, M. G.; McDermott, A. *J. Am. Chem. Soc.* **1994**, *116*, 8362–8363.
- (82) Zysmilich, M. G.; McDermott, A. *Proc. Natl. Acad. Sci. U.S.A.* **1996**, *93*, 6857–6860.
- (83) Liu, K.; Williams, J.; Lee, H.; Fitzgerald, M. M.; Jensen, G. M.; Goodin, D. B.; McDermott, A. E. *J. Am. Chem. Soc.* **1998**, *120*, 10199–10202.
- (84) Lee, H.; Ortiz de Montellano, P. R.; McDermott, A. E. *Biochemistry* **1999**, *38*, 10808–10813.
- (85) Albert, A. D.; Watts, A.; Spooner, P.; Groebner, G.; Young, J.; Yeagle, P. L. *Biochim. Biophys. Acta* **1997**, *1328*, 74–82.
- (86) Spooner, P. J. R.; Veenhoff, L. M.; Watts, A.; Poolman, B. *Biochemistry* **1999**, *38*, 9634–9639.
- (87) Jovanovic, T.; McDermott, A. E. *J. Am. Chem. Soc.* **2005**, *127*, 13816–13821.
- (88) Buffy, J. J.; Hong, T.; Yamaguchi, S.; Waring, A. J.; Lehrer, R. I.; Hong, M. *Biophys. J.* **2003**, *85*, 2363–2373.
- (89) Su, Y.; Mani, R.; Hong, M. *J. Am. Chem. Soc.* **2008**, *130*, 8856–8864.
- (90) Wickramasinghe, N. P.; Koteka, M.; Samoson, A.; Past, J.; Ishii, Y. *J. Magn. Reson.* **2007**, *184*, 350–356.
- (91) Linser, R.; Chevelkov, V.; Diehl, A.; Reif, B. *J. Magn. Reson.* **2007**, *189*, 209–216.
- (92) Wickramasinghe, N. P.; Parthasarathy, S.; Jones, C. R.; Bhardwaj, C.; Long, F.; Koteka, M.; Mehboob, S.; Fung, L. W. M.; Past, J.; Samoson, A.; Ishii, Y. *Nature Methods* **2009**, *6*, 215–218.
- (93) Balayssac, S.; Bertini, I.; Lelli, M.; Luchinat, C.; Maletta, M. *J. Am. Chem. Soc.* **2007**, *129*, 2218–2219.
- (94) Balayssac, S.; Bertini, I.; Bhaumik, A.; Lelli, M.; Luchinat, C. *Proc. Natl. Acad. Sci. U.S.A.* **2008**, *105*, 17284–17289.
- (95) Nadaud, P. S.; Helmus, J. J.; Hofer, N.; Jaroniec, C. P. *J. Am. Chem. Soc.* **2007**, *129*, 7502–7503.

ing the intensities of cross peaks in conventional 2D ^{15}N – ^{13}C SSNMR chemical shift correlation spectra—which are modulated according to the magnitudes of transverse ^1H , ^{13}C , and ^{15}N PREs—and, although qualitative in nature, were found to correlate remarkably well with electron–nucleus distances expected based on the known three-dimensional structure of GB1. Nitroxide spin labels were purposely selected for this initial study due to the fact that they are among the strongest relaxation agents; we note here that the experimental signal intensities in our SSNMR data sets were generally consistent with transverse nuclear PRE magnitudes predicted using eq 2 with $T_{1e} \approx 100$ ns, which is on the order of the T_{1e} values typically reported in the context of solution-state NMR experiments.^{55,60} While such transverse PRE-based attenuation of signal intensities in fingerprint 2D or 3D SSNMR correlation spectra is a valuable tool for certain types of applications, including rapid assessment of the overall protein topology, spectral editing, and detection of intermolecular interactions, the use of nitroxides as relaxation agents has a potentially significant drawback in the context of high-resolution protein structure refinement. Namely, quantitative measurements of nuclear PREs, and hence electron–nucleus distances, are difficult or impossible to perform for a number of protein sites due to low and/or missing spectral intensities; indeed, straightforward estimates of transverse ^1H , ^{13}C , and ^{15}N magnetization decay based on eq 2 indicate that even for 2D ^{15}N – ^{13}C cross polarization (CP) based SSNMR experiments of the shortest possible duration, cross peaks arising from residues found within ~ 10 Å of the spin label are likely to be effectively attenuated to the level of random noise.⁵⁵ Thus, in order to facilitate comprehensive, quantitative SSNMR measurements of electron–nucleus distances in paramagnetic proteins, the ability to appropriately tune (in this case reduce) the magnitude of transverse nuclear PREs would be highly desirable. Inspection of eq 2 suggests that PRE tuning of this type may be experimentally possible to achieve by introducing, instead of nitroxides, paramagnetic relaxation agents that exhibit different electronic properties. Cu^{2+} ions appear to be among the most attractive choices in this regard, because they are characterized by $S = 1/2$ in analogy to spin labels but at the same time exhibit T_{1e} 's that are reduced by ~ 1 – 2 orders of magnitude, with typical values in the ~ 1 – 5 ns range.⁵⁵ This implies that, for a fixed electron–nucleus distance and particular nucleus type, transverse PREs due to a Cu^{2+} center should be reduced by a factor of ~ 20 – 100 relative to a nitroxide spin label depending on the precise T_{1e} values, suggesting that signals from nuclei as close as ~ 5 – 6 Å to the Cu^{2+} ion may be readily detectable by standard SSNMR methods.

Here we explore this possibility of modulating the nuclear relaxation rates in MAS SSNMR spectra of natively diamagnetic uniformly ^{13}C , ^{15}N -enriched proteins via the incorporation at specific sites of covalently attached tags containing paramagnetic metal ions, with the ultimate goal of extracting electron–nucleus distance restraints for most residues by using quantitative measurements of nuclear PREs. We demonstrate this approach for the K28C and T53C mutants of GB1, where the paramagnetic ions are introduced as EDTA–metal complexes by modifying the cysteine side chain with a thiol-specific reagent, N –[S -(2-pyridylthio)cysteaminyl]EDTA-metal.^{96,97} The main

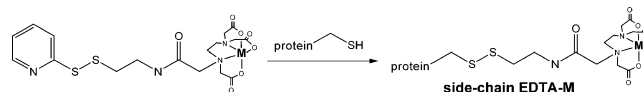


Figure 1. Modification of cysteine residues in proteins using N –[S -(2-pyridylthio)cysteaminyl]EDTA-metal,^{96,97} yielding side-chain EDTA-M ($M = \text{Cu}^{2+}$, Mn^{2+} , or Zn^{2+}).

focus of the current study is on EDTA– Cu^{2+} modified proteins; however, to further validate the approach, EDTA– Zn^{2+} and EDTA– Mn^{2+} side chains were also incorporated. The diamagnetic Zn^{2+} ion serves as an important negative control, required for the most accurate quantification of nuclear PREs, while the paramagnetic Mn^{2+} center ($S = 5/2$, $T_{1e} \approx 10$ ns⁵⁵) is anticipated to display significant differences relative to Cu^{2+} and generate large transverse nuclear PREs, similar in magnitude to those caused by nitroxide spin labels.

Experimental Section

Protein Expression and Purification. The GB1 plasmid DNA was kindly provided by Dr. Angela M. Gronenborn (University of Pittsburgh), and the plasmids encoding for the K28C and T53C mutants of GB1 were described in ref 95. Proteins were expressed in *Escherichia coli* in Luria–Bertani medium (for proteins at natural abundance) or a minimal medium containing 1 g/L $^{15}\text{NH}_4\text{Cl}$ and 3 g/L ^{13}C -glucose (for uniformly ^{13}C , ^{15}N -enriched proteins), and purified by using a combination of heat treatment at 80 °C and size exclusion chromatography.⁹⁵ The proteins were routinely characterized by SDS-PAGE, MALDI-TOF mass spectrometry and solution-state NMR spectroscopy.

Incorporation of EDTA–Metal Side Chains. Paramagnetic Mn^{2+} or Cu^{2+} ions, as well as diamagnetic Zn^{2+} , were incorporated into K28C-GB1 and T53C-GB1 as EDTA–metal complexes,^{96,97} by using a thiol-specific disulfide reagent, N –[S -(2-pyridylthio)cysteaminyl]EDTA, purchased from Toronto Research Chemicals (Toronto, ON, Canada) and preloaded with the appropriate metal ion (Figure 1). The modified proteins are referred to as 28EDTA-M and 53EDTA-M, with $M = \text{Cu}^{2+}$, Mn^{2+} , or Zn^{2+} . Since the most extensive set of experiments was carried out for 53EDTA-M proteins (with 28EDTA– Cu^{2+} and 28EDTA– Zn^{2+} samples, prepared in exactly the same fashion, subsequently used to confirm the major findings), below we focus on the preparation and characterization of 53EDTA-M samples and refer to the results for 28EDTA– Cu^{2+} / Zn^{2+} where appropriate.

A solution of T53C-GB1 in 50 mM sodium phosphate pH 6.5 buffer, containing 150 mM NaCl and 5 mM dithiothreitol (DTT) was eluted through a series of five HiTrap 5 mL desalting columns (GE Healthcare Bio-Sciences, Piscataway, NJ) equilibrated with 50 mM sodium phosphate at pH 6.5. Immediately thereafter, the protein was incubated overnight at 4 °C with a 5-fold molar excess of N –[S -(2-pyridylthio)cysteaminyl]EDTA, delivered as an aqueous solution and preloaded with 1.1 mol equiv of Cu^{2+} , Mn^{2+} , or Zn^{2+} by using $\text{CuCl}_2 \cdot 2\text{H}_2\text{O}$ (99.999%; Sigma-Aldrich, St. Louis, MO), MnCl_2 (99.999%; Sigma-Aldrich), or ZnCl_2 (99.999%; Sigma-Aldrich). Excess N –[S -(2-pyridylthio)cysteaminyl]EDTA-metal was removed by extensive buffer exchange with 50 mM sodium phosphate at pH 6.5 using an Amicon Ultra-15 3,000 molecular weight limit centrifugal device (Millipore, Billerica, MA). Mass spectrometry and solution-state NMR were used to confirm the incorporation of EDTA–M side-chains.

Solution-State NMR Spectroscopy. Samples for solution-state NMR analysis consisted of 1.5 mM ^{15}N -53EDTA-M in H_2O solution containing 50 mM sodium phosphate and 7% D_2O at pH 6.5 in a total volume of 500 μL . Two-dimensional ^1H – ^{15}N heteronuclear single quantum coherence (HSQC)⁹⁸ were recorded at 25 °C using a 600 MHz Bruker spectrometer equipped with a triple resonance three-axis pulsed field gradient probe optimized for ^1H detection. Data were processed and analyzed using NMRPipe/NMRDraw software.⁹⁹

(96) Ermácora, M. R.; Delfino, J. M.; Cuenoud, B.; Schepartz, A.; Fox, R. O. *Proc. Natl. Acad. Sci. U.S.A.* **1992**, 89, 6383–6387.

(97) Ebright, Y. W.; Chen, Y.; Pendergrast, S.; Ebright, R. H. *Biochemistry* **1992**, 31, 10664–10670.

Preparation of Paramagnetic Protein Samples for Solid-State NMR Studies

The microcrystalline paramagnetic protein samples for SSNMR analysis consisted of ^{13}C , ^{15}N -53EDTA- Cu^{2+} /Mn $^{2+}$ coprecipitated with diamagnetic, natural abundance (na) wild-type (wt) GB1. This was done to minimize the effects of intermolecular electron–nucleus dipolar interactions on the SSNMR spectra; the rationale for using wt GB1 as the diamagnetic matrix protein (as opposed to na-53EDTA-Zn $^{2+}$) is discussed in the Results and Discussion section below. In addition, a diamagnetic ^{13}C , ^{15}N -53EDTA-Zn $^{2+}$ control sample was made in the same manner. The samples were prepared as follows. Solutions of ^{13}C , ^{15}N -53EDTA-M ($M = \text{Cu}^{2+}$, Mn $^{2+}$, or Zn $^{2+}$) and na-GB1 were separately concentrated to ~ 30 mg/mL in 50 mM sodium phosphate pH 6.5 buffer containing 0.02% (w/v) NaN₃ using Amicon Ultra-4 3000 molecular weight limit centrifugal devices. The protein solutions were then mixed to yield a 53EDTA-M:GB1 molar ratio of $\sim 1:2.5$. Protein microcrystals were obtained by microdialysis at 4 °C, using microdialysis buttons purchased from Hampton Research (Aliso Viejo, CA) with a precipitant solution containing 2-methylpentane-2,4-diol, isopropanol, and deionized water in a 2:1:1 (v/v) ratio. The crystallization was allowed to proceed for at least 7 days, and the resulting protein microcrystals were center-packed by centrifugation into 3.2 mm Varian (Palo Alto, CA) thin-wall zirconia rotors. The amounts of ^{13}C , ^{15}N -53EDTA-M proteins in the final NMR samples were estimated to be $\sim 8 \pm 1$ mg by comparing the spectral intensities in 1D ^{13}C and ^{15}N SSNMR spectra to those in previously characterized control samples of ^{13}C , ^{15}N -GB1.

Solid-State NMR Spectroscopy. Experiments were performed on a three-channel Varian spectrometer operating at frequencies of 499.8 MHz for ^1H , 125.7 MHz for ^{13}C and 50.6 MHz for ^{15}N , and equipped with a 3.2 mm Varian BioMAS probe.¹⁰⁰ The MAS frequency was set to 11.111 kHz and regulated to ca. ± 3 Hz, and the sample temperature was controlled by using a stream of compressed air delivered to the sample at a flow rate of ~ 30 L/min through a variable-temperature stack. The compressed air temperature was set to 0 °C, resulting in an effective sample temperature of ~ 5 °C as determined by lead nitrate calibration.¹⁰¹ Typical ^1H , ^{13}C , and ^{15}N 90° pulse lengths were 2.5, 5.0, and 5.5 μs , respectively; where appropriate, additional experiment-specific parameters are provided in the text and figure captions. All NMR spectra were processed in NMRPipe⁹⁹ and analyzed using NM-Draw⁹⁹ and Sparky.¹⁰²

The 2D and 3D SSNMR pulse schemes used to establish the sequential resonance assignments of 53EDTA-M proteins included 2D $^{15}\text{N}-^{13}\text{C}\alpha$ (NCA), $^{15}\text{N}-^{13}\text{C}'$ (NCO), $^{15}\text{N}-^{(13)\text{Ca}}-^{13}\text{CX}$ (N(CA)CX), $^{15}\text{N}-^{(13)\text{C}'}-^{13}\text{CX}$ (N(CO)CX), and 3D $^{15}\text{N}-^{13}\text{C}\alpha-^{13}\text{CX}$ (NCACX), $^{15}\text{N}-^{13}\text{C}'-^{13}\text{CX}$ (NCOCX), and $^{13}\text{C}'-^{15}\text{N}-^{13}\text{C}\alpha$ (CONCA).^{19,20} The $^{15}\text{N}-^{13}\text{Ca/C}'$ and $^{13}\text{C}-^{13}\text{C}$ magnetization transfers were achieved using band-selective SPECIFIC CP¹⁰³ and radio frequency (rf) assisted proton-driven spin diffusion,^{104,105} respectively, and during indirect chemical shift evolution and acquisition periods two-pulse phase-modulated (TPPM) proton

decoupling¹⁰⁶ was applied at a rf field strength of ~ 70 kHz. The ^1H , ^{13}C , and ^{15}N rf field strengths and mixing times employed in the different experiments were analogous to those used by us and others in previous studies of this type.^{11,16,17}

Measurements of collective R_1 and $R_{1\rho}$ relaxation rates for backbone amide ^1H and ^{15}N nuclei in 53EDTA-M proteins were performed using the following pulse schemes based on $^1\text{H}-^{15}\text{N}$ CP and ^{15}N detection and containing variable delays (τ) during which longitudinal or spin-locked (SL) transverse $^1\text{H}/^{15}\text{N}$ magnetization was allowed to build up or decay, ^1H R_1 : $\pi_x(^1\text{H})-\tau-\pi/2_x(^1\text{H})-^{1\text{H}}-^{15}\text{N}$ CP_y-acquire; ^1H $R_{1\rho}$: $\pi/2_x(^1\text{H})-^{1\text{H}}$ SL_y(τ)- $^{1\text{H}}-^{15}\text{N}$ CP_y-acquire; ^{15}N R_1 : $\pi/2_x(^1\text{H})-^{1\text{H}}-^{15}\text{N}$ CP_y- $\pi/2_x(^{15}\text{N})-\tau-\pi/2_x(^{15}\text{N})$ -acquire; ^{15}N $R_{1\rho}$: $\pi/2_x(^1\text{H})-^{1\text{H}}-^{15}\text{N}$ CP_y- ^{15}N SL_y(τ)-acquire. The CP, spin-lock and ^1H decoupling parameters were the same as those used in a previous study.⁹⁵ Site-resolved ^{15}N R_1 measurements were carried out using a 2D NCA based pulse scheme^{87,107} (cf., Figure 7A), with CP parameters identical to those employed in experiments used to establish resonance assignments.

Results and Discussion

Solution-State NMR Characterization of 53EDTA-M Proteins. Prior to solid-state NMR analysis, the 53EDTA-M proteins were characterized by solution-state NMR to assess the protein fold and metal ion incorporation. Figure 2 shows small regions from 2D $^1\text{H}-^{15}\text{N}$ HSQC NMR spectra of ^{15}N -labeled 53EDTA-Zn $^{2+}$, 53EDTA-Cu $^{2+}$, and 53EDTA-Mn $^{2+}$. The comparison of residue-specific backbone amide ^1H and ^{15}N chemical shifts for 53EDTA-Zn $^{2+}$ and wt GB1 (Supporting Information, Figure S1) reveals that the vast majority are within 0.1 ppm for $^1\text{H}^N$ and 0.3 ppm for ^{15}N , with the largest shift differences observed for residues I6 ($\beta 1$ -strand), D46 ($\beta 3$ -strand), F52, and V54 ($\beta 4$ -strand) in the immediate spatial proximity of the EDTA-M side chain. These data are in agreement with our previously reported results for nitroxide spin-labeled T53C-GB1,⁹⁵ and imply that the backbone conformation of 53EDTA-Zn $^{2+}$ does not differ appreciably from that of wt GB1.

The spectra of paramagnetic 53EDTA-Mn $^{2+}$ /Cu $^{2+}$ proteins display minor pseudocontact chemical shifts relative to 53EDTA-Zn $^{2+}$ and considerable transverse PREs, particularly for Mn $^{2+}$ (Figure 2C), which lead to attenuated cross-peak intensities for nuclei in the vicinity of the EDTA-M side chain. These results are consistent with the fact that Mn $^{2+}$ and Cu $^{2+}$ ions are characterized by small g-tensor anisotropies and relatively large T_{1e} relaxation times in the nanosecond regime.⁵⁵ Moreover, the fact that residues found in strands $\beta 1$, $\beta 3$, and $\beta 4$ experience the most significant relaxation enhancements, while signals arising from nuclei in the α -helix are virtually unaffected by the presence of paramagnetic ions (Figure 2D), further supports the notion that 53EDTA-M proteins adopt the wt GB1 fold.

Preparation of Paramagnetic Protein Samples for Solid-State NMR Studies. The preparation of paramagnetic protein samples for solid-state NMR studies generally requires the consideration of both intra- and intermolecular electron–nucleus dipolar couplings.^{93–95} If measurements of intramolecular electron–nucleus distance restraints, which report on the global protein fold, are of primary interest, as is the case here, the ^{13}C , ^{15}N -labeled paramagnetic protein must be diluted in a lattice of natural abundance diamagnetic proteins in order to minimize the effects of intermolecular couplings on SSNMR spectra. This

- (98) Cavanagh, J.; Fairbrother, W. J.; Palmer, A. G.; Rance, M.; Skelton, N. J. *Protein NMR Spectroscopy: Principles and Practice*; Elsevier Academic Press: San Diego, CA, 2007.
- (99) Delaglio, F.; Grzesiek, S.; Vuister, G. W.; Zhu, G.; Pfeifer, J.; Bax, A. *J. Biomol. NMR* **1995**, *6*, 277–293.
- (100) Stringer, J. A.; Bronnimann, C. E.; Mullen, C. G.; Zhou, D. H. H.; Stellfox, S. A.; Li, Y.; Williams, E. H.; Rienstra, C. M. *J. Magn. Reson.* **2005**, *173*, 40–48.
- (101) Bielecki, A.; Burum, D. P. *J. Magn. Reson. A* **1995**, *116*, 215–220.
- (102) Goddard, T. D.; Kneller, D. G. SPARKY 3; University of California, San Francisco; <http://www.cgl.ucsf.edu/home/sparky>.
- (103) Baldus, M.; Petkova, A. T.; Herzfeld, J.; Griffin, R. G. *Mol. Phys.* **1998**, *95*, 1197–1207.
- (104) Takegoshi, K.; Nakamura, S.; Terao, T. *Chem. Phys. Lett.* **2001**, *344*, 631–637.
- (105) Morcombe, C. R.; Gaponenko, V.; Byrd, R. A.; Zilm, K. W. *J. Am. Chem. Soc.* **2004**, *126*, 7196–7197.
- (106) Bennett, A. E.; Rienstra, C. M.; Auger, M.; Lakshmi, K. V.; Griffin, R. G. *J. Chem. Phys.* **1995**, *103*, 6951–6957.
- (107) Giraud, N.; Bockmann, A.; Lesage, A.; Penin, F.; Blackledge, M.; Emsley, L. *J. Am. Chem. Soc.* **2004**, *126*, 11422–11423.
- (108) Koradi, R.; Billeter, M.; Wuthrich, K. *J. Mol. Graph.* **1996**, *14*, 51–55.

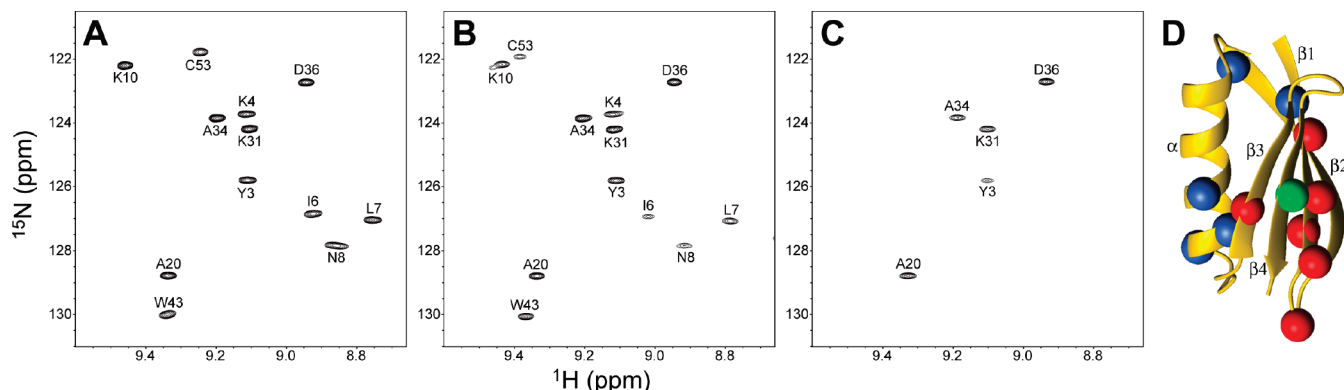


Figure 2. Small regions from ¹H-¹⁵N HSQC NMR spectra of 1.5 mM ¹⁵N-labeled 53EDTA-Zn²⁺ (A), 53EDTA-Cu²⁺ (B), and 53EDTA-Mn²⁺ (C). (D) Ribbon diagram of GB1 (PDB entry 1PGA), with the EDTA-M site indicated by a green sphere on the C α atom of residue 53. Residues other than C53 exhibiting the largest transverse PREs in the spectral region shown in panels (B,C) are indicated by red spheres and include K4, I6, L7, N8, K10, and W43. Residues exhibiting less pronounced transverse relaxation effects (Y3, A20, K31, A34, and D36) are indicated by blue spheres. The figure was prepared using MOLMOL.¹⁰⁸

can usually be achieved by precipitation of a solution containing a mixture of the paramagnetic protein and its diamagnetic analogue; paramagnetic-to-diamagnetic molar ratios of ~1:3 appear to provide a reasonable compromise between the effective attenuation of intermolecular couplings and acceptable signal-to-noise ratio for the SSNMR experiments, as has been demonstrated for matrix metalloproteinase 12⁹⁴ and nitroxide spin-labeled analogues of GB1.⁹⁵ Consequently, in the context of the current study, this strategy would call for the preparation of protein microcrystals consisting of ¹³C,¹⁵N-53EDTA-Cu²⁺/Mn²⁺ diluted in a na-53EDTA-Zn²⁺ lattice. While conceptually valid, the practical implementation of this approach suffers from a major potential drawback. This is related to the fact that despite the high affinities of Zn²⁺, Cu²⁺, and Mn²⁺ ions for EDTA, characterized by association constants in the ~10¹³-10¹⁸ regime,¹⁰⁹ metal-EDTA complexes can be relatively labile in solution,^{110,111} which may in turn lead to undesirable metal ion exchange between different types of EDTA-M proteins during the course of microcrystal formation.

In order to probe whether metal ion exchange is an important factor under our experimental crystallization conditions, we have monitored the time evolution of 2D ¹H-¹⁵N HSQC spectra for protein solutions consisting of ¹⁵N-53EDTA-Cu²⁺/Mn²⁺ and na-53EDTA-Zn²⁺ in a 1:3 molar ratio. In Figure 3 we show small regions of the spectra for ¹⁵N-53EDTA-Mn²⁺ and -Cu²⁺ recorded 1–12 h following the addition of na-53EDTA-Zn²⁺ (green contours); for reference, spectra of pure ¹⁵N-53EDTA-Mn²⁺/Cu²⁺ and ¹⁵N-53EDTA-Zn²⁺ are also shown as single blue and red contours, respectively. For both paramagnetic proteins, the appearance in the spectra of signals corresponding to ¹⁵N-53EDTA-Zn²⁺ indicates that significant metal ion scrambling between the EDTA-M side chains occurs on the time scale of minutes to hours. Figure S2 of the Supporting Information shows representative cross-peak trajectories for several residues in the vicinity of the metal binding site. These data reveal that for 53EDTA-Mn²⁺ the exchange with Zn²⁺ is completed rapidly, within ~1 h, while the Cu²⁺ and Zn²⁺ ions are fully redistributed between EDTA binding sites in ~12 h. Altogether, these results indicate that the dilution of paramagnetic 53EDTA-Mn²⁺/Cu²⁺

proteins in a 53EDTA-Zn²⁺ lattice is not feasible. Although the exchange of Zn²⁺ with Cu²⁺ is considerably slower in comparison to Mn²⁺, both paramagnetic metal ions exchange with Zn²⁺ on a time scale that is much faster than that required for microcrystal formation. Moreover, the fact that protein crystals typically contain ~30–70% solvent by volume¹¹² suggests that such metal ion exchange may also continue to occur in the microcrystalline solid phase.

To overcome the problems associated with the scrambling of metal ions upon mixing of paramagnetic 53EDTA-Mn²⁺/Cu²⁺ proteins with 53EDTA-Zn²⁺, we have pursued the use of wt na-GB1, which does not contain any high-affinity metal binding sites, as the diamagnetic alternative to 53EDTA-Zn²⁺. Solution-state NMR studies analogous to those presented in Figure 3 reveal that the addition of excess na-GB1 to ¹⁵N-53EDTA-Mn²⁺/Cu²⁺ has no effect on the ¹H-¹⁵N HSQC spectra (data not shown), indicating that Mn²⁺ and Cu²⁺ ions are chelated only by EDTA side chains. In order to probe if GB1 and 53EDTA-M proteins cocrystallize within the same homogeneous lattice, we have investigated, by 2D ¹⁵N-¹³C α SSNMR correlation spectroscopy, protein microcrystals formed by na-53EDTA-Zn²⁺ or Mn²⁺, and ¹³C,¹⁵N-GB1 in a 1:3 molar ratio (these samples were prepared using procedures analogous to those described in the Experimental Section). The SSNMR spectra of these mixed 53EDTA-M/GB1 crystals, shown in Figure 4, reveal that several well-resolved and easily identifiable residues in GB1¹¹ (V29, G38, and D40) experience large transverse PREs in the sample containing 53EDTA-Mn²⁺ (Figure 4B) relative to the 53EDTA-Zn²⁺ control (Figure 4A). Such PRE effects can arise only from intermolecular contacts between neighboring protein molecules in the crystal lattice, thereby indicating that GB1 and 53EDTA-M form sufficiently homogeneous mixed crystals and validating the use of wt GB1 as the diamagnetic matrix protein in this study.

Modulation of Nuclear Relaxation Rates in the Solid Phase by Paramagnetic Ions. With the protocol for the preparation of EDTA-M protein microcrystals for SSNMR studies established, we made samples of ¹³C,¹⁵N-53EDTA-Cu²⁺, -Mn²⁺, and -Zn²⁺ diluted in a na-GB1 lattice as described in the Experimental Section. Figure 5 shows the 2D NCA spectra for these 53EDTA-M proteins, with the ¹⁵N-¹³C α correlations labeled by residue number in the 53EDTA-Zn²⁺ spectrum

- (109) Martell, A. E.; Smith, R. M. *Critical Stability Constants*; Plenum Press: New York, 1974; Vol. 1.
 (110) Hughes, V. L.; Martell, A. E. *J. Phys. Chem.* **1953**, *57*, 694–699.
 (111) Kula, R. J.; Sawyer, D. T.; Chan, S. I.; Finley, C. M. *J. Am. Chem. Soc.* **1963**, *85*, 2930–2936.

- (112) Matthews, B. W. *J. Mol. Biol.* **1968**, *33*, 491–497.

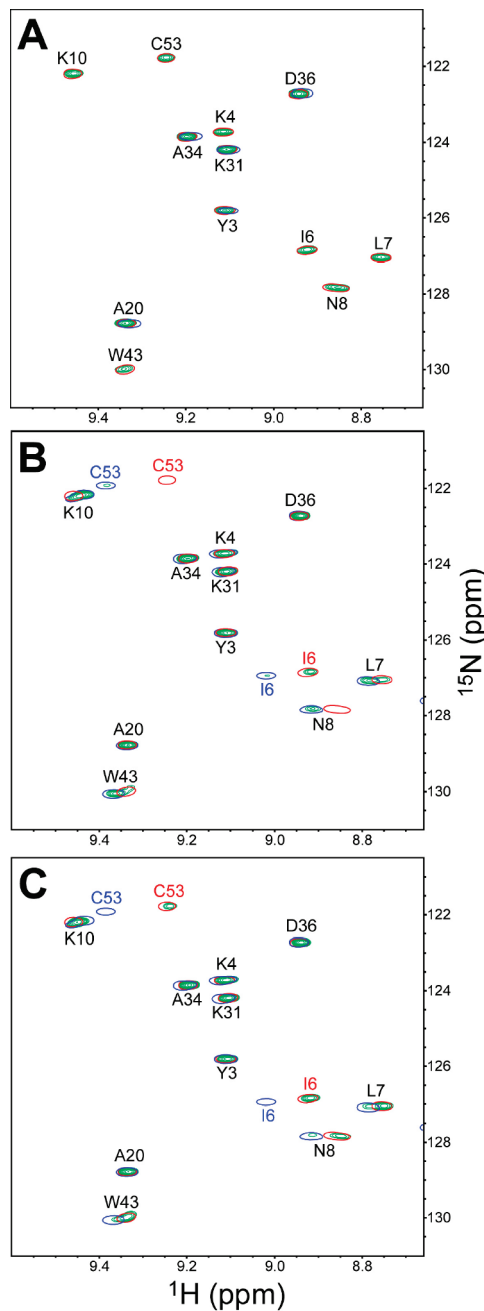


Figure 3. Observation of metal ion exchange in solution upon mixing of 53EDTA-M proteins. Shown are small regions from 2D ^1H - ^{15}N HSQC spectra of 1.5 mM ^{15}N -53EDTA- Mn^{2+} (A), and ^{15}N -53EDTA- Cu^{2+} (B,C) obtained before (single blue contours; cf., Figure 2B,C) and (A) 1 h, (B) 2 h, and (C) 12 h after the addition of a 3-fold molar excess of na-53EDTA- Zn^{2+} (green contours). For reference, the spectrum of ^{15}N -53EDTA- Zn^{2+} is also shown in panels (A–C) as a single red contour (cf., Figure 2A).

(Figure 5A). Complete backbone assignments were established for 53EDTA- Zn^{2+} by using a set of 2D and 3D correlation spectra noted in the Experimental Section (see Supporting Information Figure S3 for representative strips from the 3D NCACX, NCOCX and CONCA data sets). As is the case in solution (cf., Figure 2), 53EDTA- Mn^{2+} and - Cu^{2+} do not display appreciable pseudocontact shifts in the solid phase—this allows the resonances in 2D NCA spectra for these proteins to be assigned in a straightforward manner, by mapping the observed cross peaks directly onto the 53EDTA- Zn^{2+} NCA spectrum. The validity of this approach was further confirmed by recording

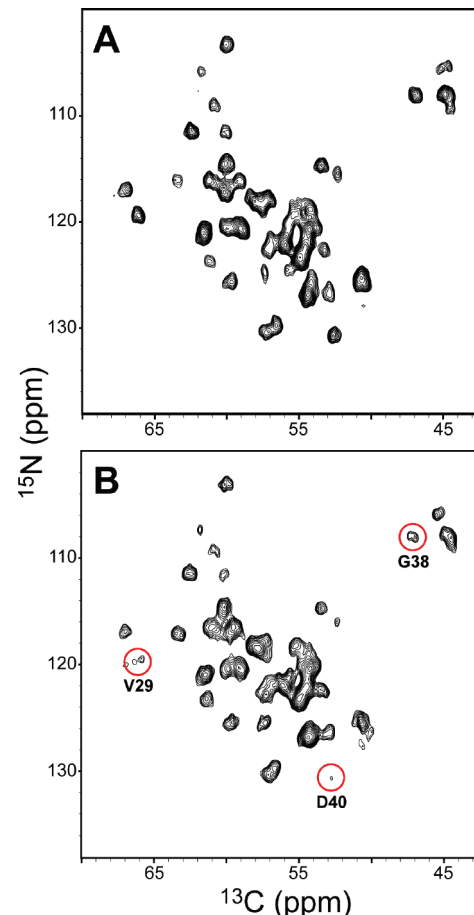


Figure 4. 500 MHz 2D ^{15}N - ^{13}C solid-state NMR spectra of ^{13}C , ^{15}N -GB1 cocrystallized with na-53EDTA- Zn^{2+} (A) and na-53EDTA- Mn^{2+} (B) in a 3:1 molar ratio. Spectra were recorded at 11.111 kHz MAS as 750* (t_1 , ^{15}N) \times 1250* (t_2 , ^{13}C) data matrices with time increments of (20, 20) μs resulting in acquisition times of (15, 25) ms and a total measurement time of \sim 40 h per spectrum. The lowest contours are drawn at \sim 10 times the root-mean-squared (rms) noise level. Several well-resolved resonances (V29, G38, and D40) observed in the control spectrum in (A) but largely suppressed in (B) due to intermolecular transverse PREs are labeled and highlighted by red circles.

the full set of 3D correlation spectra for 53EDTA- Cu^{2+} (data not shown) and comparing all the backbone ^{15}N and ^{13}C chemical shifts to those of 53EDTA- Zn^{2+} .

The spectra for 53EDTA- Cu^{2+} and - Mn^{2+} display remarkable differences as a result of the very different properties of the two paramagnetic centers⁵⁵ ($S = 1/2$, $T_{1e} \approx 1\text{--}5$ ns for Cu^{2+} , and $S = 5/2$, $T_{1e} \approx 10$ ns for Mn^{2+}). Specifically, due to its larger values of S and T_{1e} , the Mn^{2+} ion generates considerable transverse nuclear PREs (cf., eq 2), which lead to severe attenuation of cross-peak intensities for \sim 50% of the amino acid residues as seen qualitatively in Figure 5C; a quantitative analysis of cross-peak intensities as a function of residue number is presented in Figure S4 of the Supporting Information. As expected, nuclei closest to the Mn^{2+} center experience the largest PREs, and those further removed are relatively unaffected. For example, the most intense cross peaks in the spectrum arise from amino acids V21 (loop between β 2-strand and the α -helix), T25 and V29 (both in the α -helix), while correlations corresponding to I6 (β 1-strand), T49 (loop connecting strands β 3 and β 4) and E56 (β 4-strand) are suppressed to the level of random noise. Such transverse PRE-based attenuation of cross-peak intensities provides qualitative structural information,

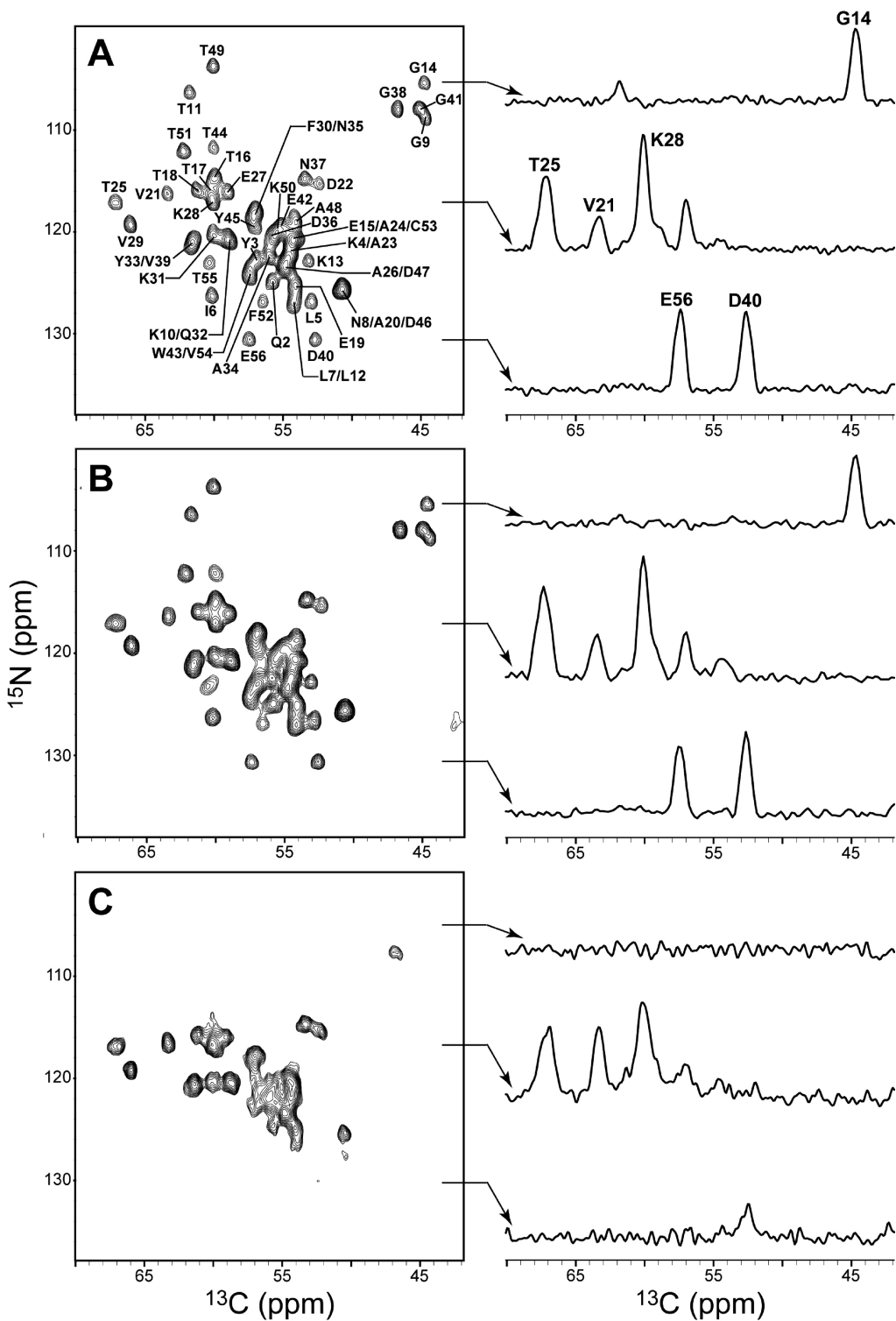


Figure 5. 500 MHz 2D ¹⁵N-¹³C α solid-state NMR spectra of (A) ¹³C,¹⁵N-53EDTA-Zn²⁺, (B) 53EDTA-Cu²⁺, and (C) 53EDTA-Mn²⁺ cocrystallized with na-GB1 in a ~1:2.5 molar ratio. Spectra were recorded at 11.111 kHz MAS as 750*(t_1 , ¹⁵N) \times 1250*(t_2 , ¹³C) data matrices with time increments of (20, 20) μ s resulting in acquisition times of (15, 25) ms; total measurement times were 17–25 h per 2D. The lowest contours are drawn at 25 (A,B) and 10 (C) times the rms noise level, with representative 1D slices corresponding to ¹⁵N frequencies of 105.2 ppm (G14), 117.1 ppm (T25/K28) and 130.8 ppm (D40/E56) shown to the right of each spectrum. Resonance assignments for 53EDTA-Zn²⁺ are indicated (see text for details).

where signals arising from residues within \sim 10–15 Å of the Mn²⁺ ion are effectively suppressed; we note here that analogous results have been obtained previously for proteins modified with covalently bound nitroxide spin labels,⁹⁵ for which $S = 1/2$ and $T_{1e} \approx 100$ ns.⁵⁵ On the other hand, all resonances in the 2D NCA spectrum of 53EDTA-Cu²⁺ (Figure 5B) display similar

widths and intensities to the corresponding signals for the 53EDTA-Zn²⁺ diamagnetic control sample, as illustrated by the 1D ¹³C traces in Figure 5 and the plot of cross-peak intensities as a function of residue number in Figure S4. This implies that transverse PRE effects are substantially attenuated for the Cu²⁺ center relative to Mn²⁺, as predicted by eq 2.

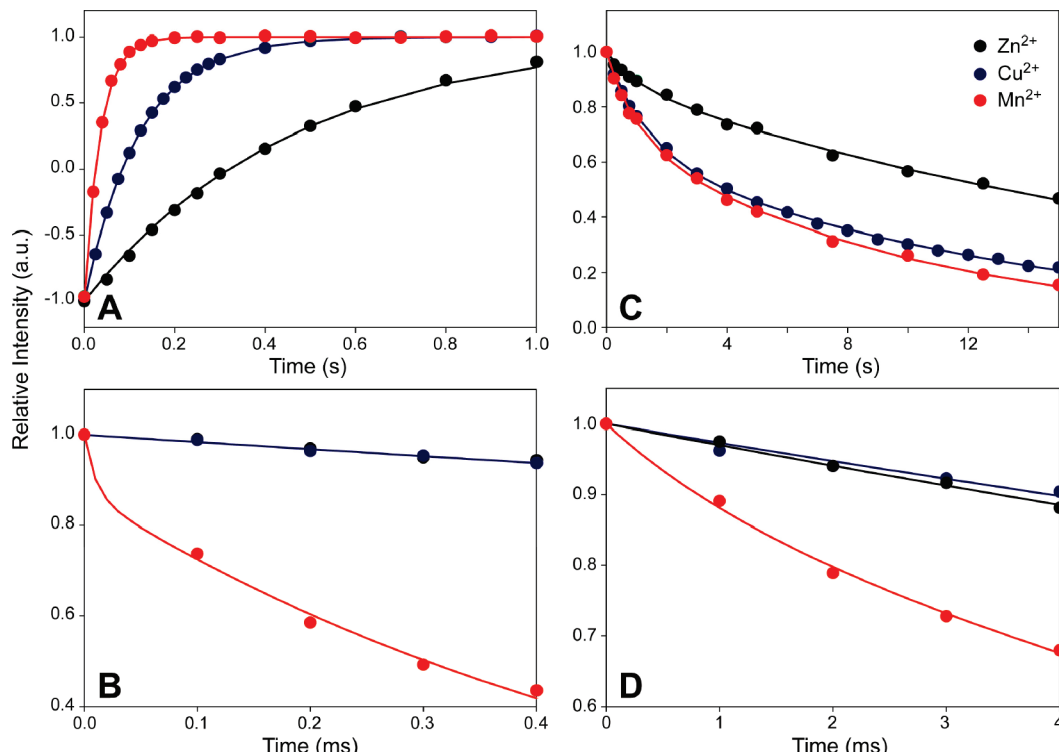


Figure 6. Measurements of collective R_1 (A,C) and $R_{1\rho}$ (B,D) relaxation rates in the solid phase for backbone amide ^1H (A,B) and ^{15}N (C,D) nuclei in 53EDTA- Zn^{2+} (black circles), 53EDTA- Cu^{2+} (blue circles), and 53EDTA- Mn^{2+} (red circles). Also shown are best fits to rising (A) or decaying (B–D) exponentials; single-exponential fits were sufficient for all data sets except ^{15}N R_1 for 53EDTA- Cu^{2+} and 53EDTA- Mn^{2+} , and $^1\text{H}/^{15}\text{N}$ $R_{1\rho}$ for 53EDTA- Mn^{2+} , which required the use of double exponentials.

To further probe the modulation of nuclear relaxation rates by paramagnetic Mn^{2+} and Cu^{2+} ions, we performed measurements of collective longitudinal (R_1) and transverse ($R_{1\rho}$) relaxation rates for amide ^1H and ^{15}N nuclei in 53EDTA-M proteins. These data, presented in Figure 6, reveal that, for the longest delays investigated (0.4 and 4 ms for ^1H and ^{15}N , respectively), transverse magnetization losses of $\sim 40\text{--}60\%$ are observed for 53EDTA- Mn^{2+} , while trajectories for 53EDTA- Cu^{2+} and 53EDTA- Zn^{2+} are nearly identical and do not display significant magnetization decay (Figure 6B,D). This implies that the large transverse nuclear PREs due to the Mn^{2+} center are effectively quenched for the EDTA- Cu^{2+} side chain, in agreement with the 2D NCA spectra in Figure 5. At the same time, the trajectories in Figure 6A,C indicate that both Mn^{2+} and Cu^{2+} centers generate considerable longitudinal relaxation enhancements for ^1H and ^{15}N spins relative to the diamagnetic EDTA- Zn^{2+} side chain. The combination of negligible transverse and substantial longitudinal relaxation enhancements observed for the EDTA- Cu^{2+} side-chain is particularly favorable. On one hand, 53EDTA- Cu^{2+} is expected to effectively behave as a diamagnetic protein in the context of conventional 2D and 3D SSNMR experiments; however, it also carries valuable information about the proximities of nuclear spins to the Cu^{2+} center, encoded in the longitudinal nuclear relaxation rates. This suggests the possibility of simultaneously extracting multiple structural restraints for the vast majority of residues via quantitative, site-specific measurements of nuclear R_1 values by multidimensional SSNMR methods.

Quantitative Measurements of Longitudinal ^{15}N PREs by Solid-State NMR. In this section we describe the quantitative measurements of ^{15}N longitudinal relaxation rate constants (R_1^N) for 53EDTA- Cu^{2+} and 53EDTA- Zn^{2+} (as well as for 28EDTA- Cu^{2+} and 28EDTA- Zn^{2+} samples prepared in identical fashion),

which can be used to derive site-specific PREs due to the Cu^{2+} center. Note that while analogous measurements of ^1H and ^{13}C longitudinal PREs are also possible in principle, for fully protonated protein molecules and moderate MAS rates employed in this study the interpretation of these observables in terms of protein structure is expected to be complicated by spin diffusion phenomena;^{113,114} in contrast, spin diffusion effects are far less significant for the weakly coupled ^{15}N nuclei.¹¹⁵ The residue-specific R_1^N values were determined using the pulse scheme in Figure 7A.^{87,107} This experiment involves the acquisition of a series of 2D ^{15}N - $^{13}\text{C}\alpha$ correlation spectra as a function of a variable delay, τ , during which longitudinal ^{15}N magnetization is allowed to decay; τ values in the 0–4 s range were employed here. Representative 2D NCA spectra for 53EDTA- Cu^{2+} , corresponding to τ values of 0 and 4 s, are shown in Figure 7, B and C, respectively, and analogous spectra for 28EDTA- Cu^{2+} are presented in Figure S5 of the Supporting Information. These data clearly indicate that the ^{15}N longitudinal magnetization decay is not uniform throughout the protein, and suggest that for each residue the decay rate depends on the distance between the ^{15}N nucleus and the Cu^{2+} ion. For example, while the signals arising from residues T25 and V29 in 53EDTA- Cu^{2+} , removed from the Cu^{2+} center by at least 20 Å, are relatively intense in both $\tau = 0$ and $\tau = 4$ s spectra, the cross peaks corresponding to I6 and E56, found in the immediate vicinity of the EDTA- Cu^{2+} side chain, are significantly attenuated for $\tau = 4$ s. (The converse is true for 28EDTA- Cu^{2+} , where signals arising from the α -helical residues T25 and V29 are significantly attenuated, while the I6 and E56 resonances are relatively unaffected by

(113) Bloembergen, N. *Physica* **1949**, *15*, 386–426.

(114) Suter, D.; Ernst, R. R. *Phys. Rev. B* **1985**, *32*, 5608–5627.

(115) Giraud, N.; Blackledge, M.; Bockmann, A.; Emsley, L. *J. Magn. Reson.* **2007**, *184*, 51–61.

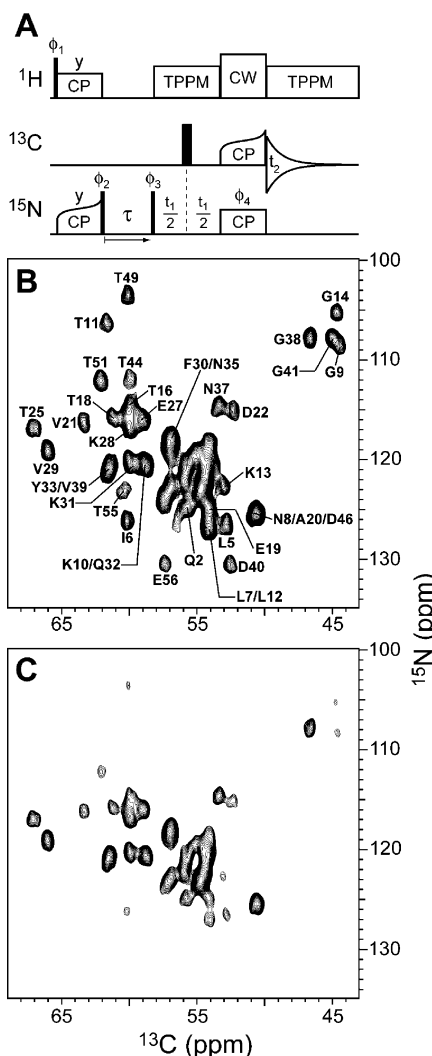


Figure 7. (A) Solid-state NMR pulse scheme for site-resolved measurements of ^{15}N R_1 values.^{87,107} The experiment involves the acquisition of a series of 2D ^{15}N - ^{13}C correlation spectra, as a function of delay τ . Narrow and wide black rectangles correspond to 90° and 180° pulses, respectively, and have phase x unless indicated otherwise. Phase cycling: $\phi_1 = 2(x)$, $2(-x)$; $\phi_2 = 4(x)$, $4(-x)$; $\phi_3 = x$, $-x$; $\phi_4 = y$; receiver = x , $-x$, $-x$, x , x , $-x$. States phase cycling of ϕ_4 is used for quadrature detection in the ^{15}N dimension.¹¹⁶ Spectra for different τ values are acquired in an interleaved manner. (B) Reference ($\tau = 0$) 2D NCA spectrum of 53EDTA-Cu²⁺ with selected assignments indicated (see Figure 5 caption for additional details). (C) 2D NCA spectrum of 53EDTA-Cu²⁺ with $\tau = 4$ s.

the presence of the paramagnetic side chain.) Indeed, the $\tau = 4$ s spectrum for 53EDTA-Cu²⁺ (Figure 7C) closely resembles the 2D NCA spectrum for 53EDTA-Mn²⁺ (Figure 5C). This implies that, as expected, residues exhibiting the largest transverse nuclear PREs due to the Mn²⁺ center, also display the largest longitudinal ^{15}N PREs in the presence of Cu²⁺.

To quantitatively determine the residue-specific longitudinal ^{15}N PREs, generated by the Cu²⁺ center, we recorded the complete ^{15}N R_1 relaxation trajectories (with $\tau = 0, 0.5, 1, 2, 3$, and 4 s) for 53EDTA-Cu²⁺/Zn²⁺ and 28EDTA-Cu²⁺/Zn²⁺. R_1^N data could be readily obtained for 21 residues in 53EDTA-Cu²⁺/Zn²⁺ and 25 residues in 28EDTA-Cu²⁺/Zn²⁺ that yielded cross peaks free of overlap in the 2D NCA spectra. Representative R_1^N trajectories for nine residues in 53EDTA-Cu²⁺/Zn²⁺ are

shown in Figure 8, where each trajectory was normalized according to the corresponding cross-peak intensity in the $\tau = 0$ spectrum; representative trajectories for 28EDTA-Cu²⁺/Zn²⁺ are shown in Figure S6 of the Supporting Information. To obtain the residue-specific R_1^N values, the trajectories were modeled using decaying single exponentials, $I(\tau) = \exp(-R_1^N\tau)$, where $I(\tau)$ is the relative cross-peak intensity at time τ ; we note that the single-exponential model provided a reasonable description for all the trajectories, with the largest discrepancies observed for residues T55 and E56 in 53EDTA-Cu²⁺. The R_1^N values in 53EDTA-Zn²⁺ and 28EDTA-Zn²⁺ were found to vary by more than a factor of 20, ranging from ca. 0.02 s^{-1} (for T25 in 53EDTA-Zn²⁺) to 0.43 s^{-1} (for G41 in 28EDTA-Zn²⁺). On average, the largest R_1^N values were obtained for the loop residues (T11, V21, D22, N37, G38, D40, G41, T49; $\langle R_1^N \rangle = 0.14 \pm 0.10\text{ s}^{-1}$ for both 53EDTA-Zn²⁺ and 28EDTA-Zn²⁺), while the remaining residues, located in regular elements of secondary structure, yielded lower R_1^N values with $\langle R_1^N \rangle = 0.062 \pm 0.024\text{ s}^{-1}$. These results are in good agreement with previous SSNMR measurements of backbone amide ^{15}N R_1 rate constants for the Crh protein in microcrystalline form.¹⁰⁷

In comparison with the diamagnetic 53EDTA-Zn²⁺ and 28EDTA-Zn²⁺ proteins, R_1^N values for 53EDTA-Cu²⁺ and 28EDTA-Cu²⁺ are found to be substantially higher on average, as seen readily from the rapid decay of ^{15}N longitudinal magnetization for a number of residues in Figures 8 and S6, and exhibit a greater spread ($\langle R_1^N \rangle = 0.20 \pm 0.15\text{ s}^{-1}$). In fact, all R_1^N rate constants in 53EDTA-Cu²⁺ and 28EDTA-Cu²⁺ are larger than the corresponding values in 53EDTA-Zn²⁺ and 28EDTA-Zn²⁺, respectively. Consequently, for each residue the difference between the EDTA-Cu²⁺ and EDTA-Zn²⁺ R_1^N rates, $\Gamma_1^N = R_1^N(\text{Cu}^{2+}) - R_1^N(\text{Zn}^{2+})$, yields the longitudinal ^{15}N PRE (see Table 1 and Supporting Information, Table S1). These ^{15}N PREs, which are in the range of ca. $0.01\text{--}0.8\text{ s}^{-1}$, are shown in Figure 9 as a function of residue number and location within the tertiary protein structure for 53EDTA-Cu²⁺ and 28EDTA-Cu²⁺. As qualitatively implied by the 2D NCA spectra in Figures 7 and S5, the magnitude of Γ_1^N for each residue indeed appears to be highly correlated with the distance between the corresponding ^{15}N nucleus and the Cu²⁺ center. Specifically, most residues located in the four β -strands and intervening loops of 53EDTA-Cu²⁺ exhibit the largest PRE effects ($\Gamma_1^N > 0.1\text{ s}^{-1}$), while considerably smaller PREs ($\Gamma_1^N < 0.05\text{ s}^{-1}$) are observed for residues in the α -helix and adjacent loops. On the other hand, for 28EDTA-Cu²⁺ the α -helical residues display by far the highest Γ_1^N values.

The quantitative measurements of residue-specific Γ_1^N values permit the distances between individual amide ^{15}N nuclei and the Cu²⁺ ion, $r_{\text{N}-\text{Cu}}$, to be estimated by using eq 1. In this study, these calculations yielded ^{15}N -Cu²⁺ distances between ~ 11 and 24 \AA (see Tables 1 and S1 for details); note, however, that with typical uncertainties of $\sim 0.01\text{--}0.02\text{ s}^{-1}$ for R_1^N , reliable quantitative distance estimates can be obtained only for $r_{\text{N}-\text{Cu}} \leq \sim 20\text{ \AA}$ (i.e., Γ_1^N values of $< \sim 0.02\text{ s}^{-1}$ may be within the experimental error, and, in contrast to a quantitative distance, are therefore limited to providing a lower bound of $\sim 20\text{ \AA}$ for $r_{\text{N}-\text{Cu}}$ —a valuable structural restraint nonetheless). Interestingly, the fact that the shortest distances between the Cu²⁺ center and several ^{15}N nuclei in the α -helix and β -strand for 28EDTA-Cu²⁺ and 53EDTA-Cu²⁺, respectively, are found to be in the

(117) Rakshit, G.; Antholine, W. E.; Froncisz, W.; Hyde, J. S.; Pilbrow, J. R.; Sinclair, G. R.; Sarkar, B. *J. Inorg. Biochem.* **1985**, 25, 217–224.

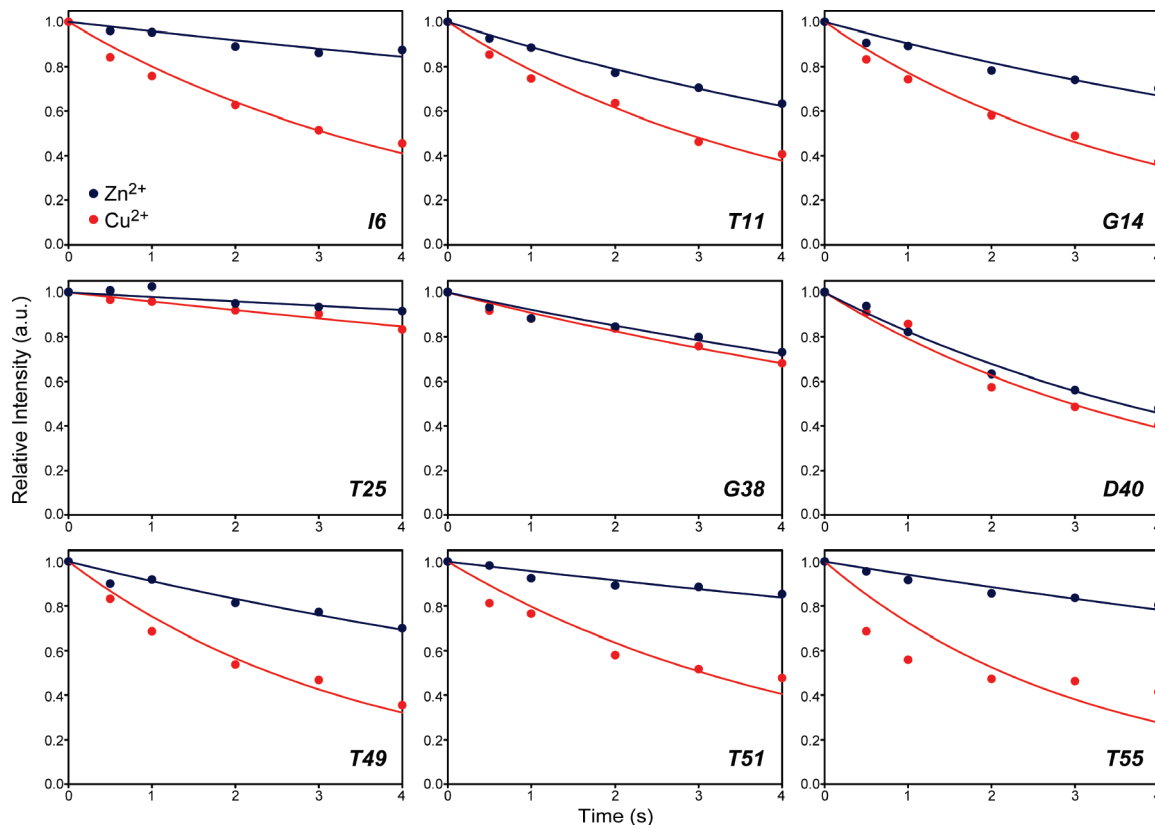


Figure 8. Representative measurements of residue-specific solid-state ^{15}N R_1 rates in 53EDTA-Zn $^{2+}$ (blue circles) and 53EDTA-Cu $^{2+}$ (red circles) obtained using the pulse scheme in Figure 7A. Best fits to decaying single exponentials are shown as solid lines.

Table 1. Backbone Amide ^{15}N Longitudinal PREs, Γ_1^N , and $^{15}\text{N}-\text{Cu}^{2+}$ Distances, $r_{\text{N}-\text{Cu}}$, Derived from R_1^N Measurements in 53EDTA-Cu $^{2+}$ and 53EDTA-Zn $^{2+}$

| residue | $R_1^N(\text{Cu}^{2+})$ (s^{-1}) | $R_1^N(\text{Zn}^{2+})$ (s^{-1}) | Γ_1^N (s^{-1}) ^a | $r_{\text{N}-\text{Cu}}$ (\AA) ^b |
|---------|---|---|---|--|
| L5 | 0.199 ± 0.020 | 0.053 ± 0.007 | 0.146 ± 0.021 | $14.3^{+0.3}_{-0.3}$ |
| I6 | 0.222 ± 0.020 | 0.043 ± 0.008 | 0.179 ± 0.022 | $13.9^{+0.3}_{-0.3}$ |
| T11 | 0.244 ± 0.016 | 0.119 ± 0.005 | 0.125 ± 0.017 | $14.7^{+0.4}_{-0.3}$ |
| K13 | 0.198 ± 0.015 | 0.091 ± 0.011 | 0.107 ± 0.019 | $15.1^{+0.3}_{-0.3}$ |
| G14 | 0.258 ± 0.018 | 0.101 ± 0.012 | 0.157 ± 0.022 | $14.2^{+0.4}_{-0.3}$ |
| T18 | 0.126 ± 0.012 | 0.097 ± 0.005 | 0.029 ± 0.013 | $18.8^{+2.0}_{-1.1}$ |
| V21 | 0.099 ± 0.007 | 0.081 ± 0.006 | 0.018 ± 0.009 | $20.3^{+2.6}_{-1.4}$ |
| D22 | 0.104 ± 0.015 | 0.075 ± 0.004 | 0.029 ± 0.016 | $18.8^{+1.9}_{-1.0}$ |
| T25 | 0.042 ± 0.004 | 0.021 ± 0.007 | 0.021 ± 0.008 | $19.8^{+1.7}_{-1.0}$ |
| E27 | 0.086 ± 0.012 | 0.056 ± 0.009 | 0.030 ± 0.015 | $18.7^{+2.3}_{-1.2}$ |
| K28 | 0.084 ± 0.003 | 0.074 ± 0.011 | 0.010 ± 0.011 | $22.4^{+2.7}_{-2.7}$ |
| V29 | 0.065 ± 0.017 | 0.055 ± 0.007 | 0.010 ± 0.018 | $22.4^{+3.6}_{-3.6}$ |
| N37 | 0.100 ± 0.018 | 0.093 ± 0.015 | 0.007 ± 0.023 | $23.8^{+5.2}_{-5.2}$ |
| G38 | 0.097 ± 0.008 | 0.081 ± 0.009 | 0.016 ± 0.012 | $20.7^{+5.4}_{-1.9}$ |
| D40 | 0.235 ± 0.022 | 0.195 ± 0.013 | 0.040 ± 0.026 | $17.8^{+3.3}_{-1.4}$ |
| T44 | 0.23 ± 0.03 | 0.056 ± 0.010 | 0.17 ± 0.03 | $13.9^{+0.3}_{-0.3}$ |
| T49 | 0.285 ± 0.028 | 0.092 ± 0.011 | 0.19 ± 0.03 | $13.7^{+0.4}_{-0.3}$ |
| T51 | 0.23 ± 0.03 | 0.044 ± 0.007 | 0.18 ± 0.03 | $13.8^{+0.4}_{-0.4}$ |
| F52 | 0.298 ± 0.018 | 0.027 ± 0.009 | 0.271 ± 0.020 | $12.9^{+0.2}_{-0.2}$ |
| T55 | 0.32 ± 0.09 | 0.062 ± 0.008 | 0.26 ± 0.09 | $13.0^{+1.0}_{-0.6}$ |
| E56 | 0.29 ± 0.08 | 0.091 ± 0.009 | 0.20 ± 0.08 | $13.6^{+1.2}_{-0.7}$ |

^a $\Gamma_1^N = R_1^N(\text{Cu}^{2+}) - R_1^N(\text{Zn}^{2+})$. ^b Estimated using eq 1 with $g = 2.09^{+1.7}_{-1.7}$ and $T_{1e} = 2.5$ ns. Note that similar results were obtained for $T_{1e} = 1$ ns or $T_{1e} = 5$ ns, with distances that were 1.4 ± 0.3 Å and 0.22 ± 0.05 Å lower, respectively, than estimates obtained with $T_{1e} = 2.5$ ns.

$\sim 11-13$ Å regime implies that the EDTA-Cu $^{2+}$ side chains in these proteins adopt relatively extended conformations, where fully extended side chains are characterized by C28/C53 $^{15}\text{N}-\text{Cu}^{2+}$ distances of ~ 14 Å. Such extended conformations appear to be highly probable given the location of residues 28 and 53 and conformations of neighboring side chains in wt GB1,

indicating that the ^{15}N PRE measurements report on structurally relevant distances. In order to further assess the validity of these ^{15}N PRE-based $^{15}\text{N}-\text{Cu}^{2+}$ distance estimates for future applications to protein structure elucidation, in Figure 10 we compare the experimental $r_{\text{N}-\text{Cu}}$ and Γ_1^N values with the corresponding values calculated from structural models of 28EDTA-M and 53EDTA-M (cf., Supporting Information, Tables S2 and S3); note that, although no high-resolution X-ray structures are currently available for either 28EDTA-M or 53EDTA-M, structural models of these proteins could be constructed within the XPLOR-NIH software package¹¹⁸ based on the available atomic coordinates of wt GB1. Overall, the experimentally observed distances and PREs are found to be strongly correlated with those calculated from the protein structural models, with rms deviations of ca. 0.04 s $^{-1}$ for Γ_1^N and 4.0 Å for $r_{\text{N}-\text{Cu}}$; this implies that the Solomon relaxation mechanism in eq 1 provides a reasonable theoretical framework for the analysis of these experiments. Indeed, a closer inspection of the correlation plots in Figure 10 reveals that the experimentally observed distances and PREs fall into two distinct classes as far as their agreement with values calculated from the structural models is concerned. Specifically, a subset of 15 measurements, corresponding to the largest calculated PREs ($\Gamma_1^N > 0.04$ s $^{-1}$) and shortest distances ($r_{\text{N}-\text{Cu}} < 18$ Å), shows excellent quantitative agreement between the measured and calculated $r_{\text{N}-\text{Cu}}$ values with a rms deviation of only ~ 0.7 Å. For the remaining measurements, the observed $r_{\text{N}-\text{Cu}}$ distances and PREs are all found to be respectively smaller and larger relative to values calculated from the protein structural models. These regular deviations corresponding to the smallest

(118) Schwieters, C. D.; Kuszewski, J. J.; Tjandra, N.; Clore, G. M. *J. Magn. Reson.* **2003**, *160*, 65–73.

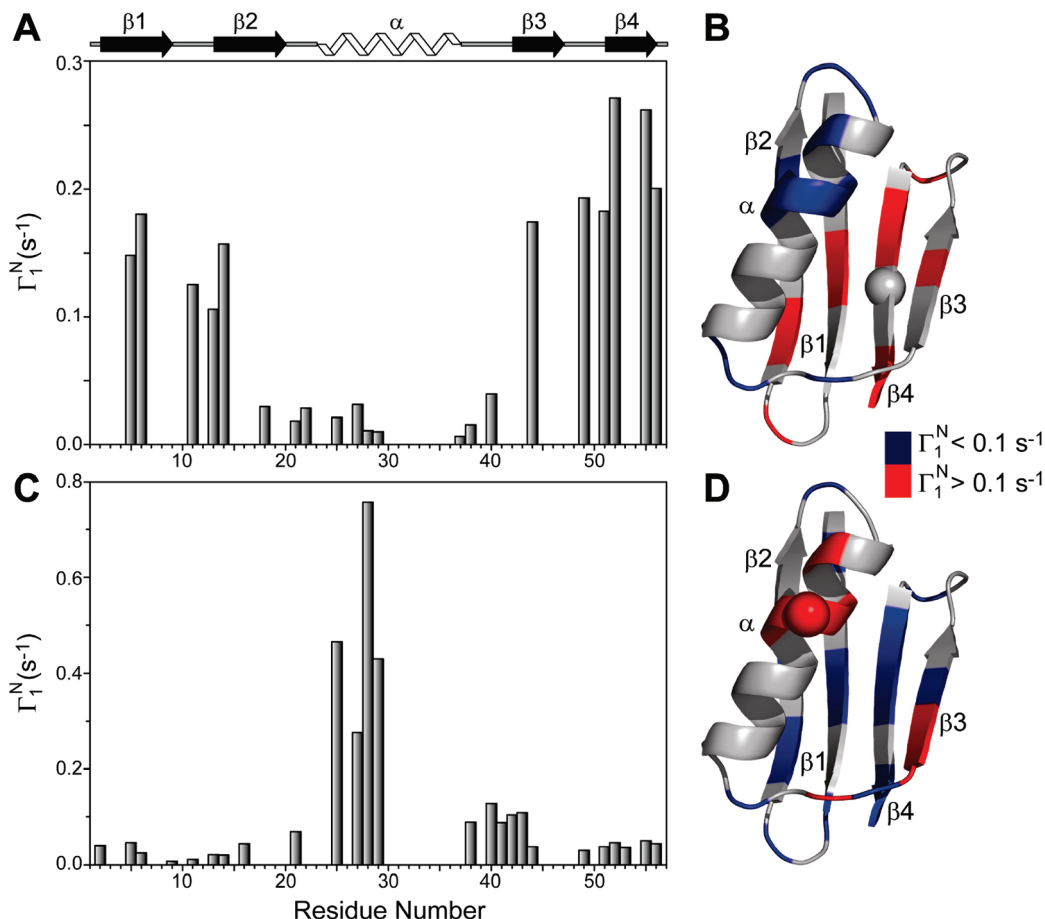


Figure 9. (A) Backbone amide ^{15}N longitudinal paramagnetic relaxation enhancements, Γ_1^N , for 53EDTA-Cu²⁺ as a function of residue number. Γ_1^N was set to zero for residues where quantitative measurements could not be made due to insufficient resolution in 2D NCA spectra. (B) Ribbon diagram of GB1 (PDB entry 1PGA), with the Γ_1^N values mapped onto the structure. Residues with $\Gamma_1^N < 0.1$ s⁻¹ ($r_{\text{N}-\text{Cu}} > \sim 15$ Å) and $\Gamma_1^N > 0.1$ s⁻¹ ($r_{\text{N}-\text{Cu}} < \sim 15$ Å) are indicated in blue and red, respectively, and residues for which Γ_1^N was not determined are colored in gray. The EDTA-Cu²⁺/Zn²⁺ incorporation site (residue 53) is indicated by a sphere on the Ca atom. (C,D) Same as panels (A,B) but for 28EDTA-Cu²⁺.

Γ_1^N values primarily reflect, in all likelihood, the residual contributions from intermolecular electron–nucleus dipolar couplings caused by the insufficient dilution of EDTA-M proteins in the diamagnetic GB1 matrix (a systematic analysis of the influence of these residual intermolecular couplings on the accurate determination of Γ_1^N and $r_{\text{N}-\text{Cu}}$ parameters will be reported elsewhere). In summary, the fact that the SSNMR measurements of ^{15}N longitudinal PREs enable quantitative estimates of multiple long-range ^{15}N –Cu²⁺ distances to be simultaneously obtained in a relatively straightforward manner bodes well for the future application of these types of restraints to protein structure refinement.

Conclusions

Using the K28C and T53C mutants of GB1 as models, we have shown that modification of natively diamagnetic proteins with covalently attached EDTA tags containing paramagnetic Mn²⁺ or Cu²⁺ ions permits the acquisition of high-resolution MAS solid-state NMR spectra and extraction of multiple long-range structural restraints. This methodology is expected to be generally applicable to peptides and proteins of varying size and complexity that contain no native cysteines and into which a solvent-exposed cysteine residue can be introduced via site-

directed mutagenesis.^{96,97,119} For protein systems that cannot accommodate such non-native cysteines, alternative approaches based on different types of metal binding tags^{120–122} or genetic encoding of metal-ion chelating amino acids¹²³ may also be used to incorporate Cu²⁺ or Mn²⁺ ions in site-specific fashion.

The information about electron–nucleus distances is encoded in the magnitudes of longitudinal and transverse nuclear relaxation rates, which, according to the Solomon relaxation mechanism, also depend on the nucleus type, electron spin–lattice relaxation time constant, T_{1e} , and spin quantum number, S . This enables relaxation rates of the protein nuclei to be appropriately tuned by incorporating paramagnetic centers with different electronic properties. Here we demonstrate that Mn²⁺ ions, characterized by relatively large values of S and T_{1e} , cause substantial transverse paramagnetic relaxation enhancements for the backbone ^1H , ^{13}C , and ^{15}N nuclei, which, in analogy to nitroxide spin labels, yield qualitative distance restraints via the

- (119) Hubbell, W. L.; Altenbach, C. *Curr. Opin. Struct. Biol.* **1994**, 4, 566–573.
- (120) Regan, L. *Annu. Rev. Biophys. Biomol. Struct.* **1993**, 22, 257–287.
- (121) Gaponenko, V.; Dvoretsky, A.; Walsby, C.; Hoffman, B. M.; Rosevear, P. R. *Biochemistry* **2000**, 39, 15217–15224.
- (122) Donaldson, L. W.; Skrynnikov, N. R.; Choy, W. Y.; Muhandiram, D. R.; Sarkar, B.; Forman-Kay, J. D.; Kay, L. E. *J. Am. Chem. Soc.* **2001**, 123, 9843–9847.
- (123) Lee, H. S.; Spraggon, G.; Schultz, P. G.; Wang, F. *J. Am. Chem. Soc.* **2009**, 131, 2481–2483.

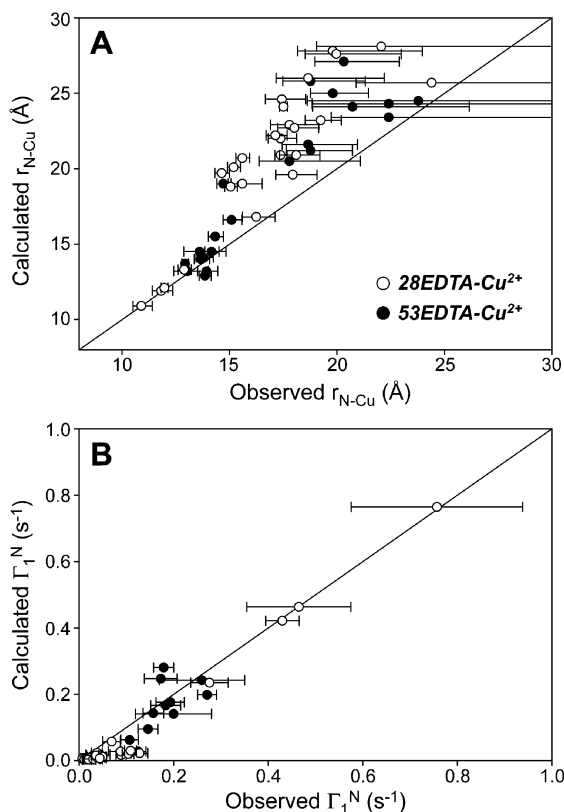


Figure 10. Comparison between the experimentally observed (A) r_{N-Cu} and (B) Γ_1^N values, and the corresponding values derived from structural models of 28EDTA-M and 53EDTA-M proteins (cf., Tables S2 and S3 of the Supporting Information).

extensive attenuation of cross-peak intensities in multidimensional SSNMR chemical shift correlation spectra. In contrast, transverse nuclear PREs are significantly reduced—indeed, effectively quenched—for the Cu²⁺ center due to the combination of its smaller S and T_{1e} parameters and the fact that the EDTA side-chain positions the Cu²⁺ ion over 10 Å away from the protein backbone.

Concurrently, both Mn²⁺ and Cu²⁺ centers are found to generate relatively large longitudinal nuclear PREs. The combination of negligible transverse and considerable longitudinal PREs obtained with the EDTA-Cu²⁺ side chain is particularly advantageous, because it enables quantitative electron–nucleus distance restraints to be obtained for most residues via site-resolved measurements of nuclear spin–lattice relaxation time constants by multidimensional SSNMR techniques. Such measurements are demonstrated here for backbone amide ¹⁵N nuclei,

revealing that longitudinal PREs are highly correlated with ¹⁵N–Cu²⁺ distances and that significant relaxation enhancements are observed for distances up to ~20 Å. While the ¹⁵N PRE measurements in this study were based on 2D ¹⁵N–¹³C α correlation spectroscopy, alternative/additional chemical shift dimensions can be readily incorporated into these experiments for increased spectral resolution. Furthermore, by performing analogous measurements of ¹³C and ¹H PREs at higher MAS rates and/or in highly deuterated proteins it may be possible to obtain additional, complementary PRE-based distance restraints involving those nuclei.

In summary, the nuclear PREs generated by Mn²⁺ or Cu²⁺ ions are capable of yielding structural information for proteins on length scales that exceed by a factor of ~3–4 the distances accessible to conventional solid-state NMR techniques. In their current form, these PRE restraints provide unique long-range information about the overall protein fold that can be used to evaluate the validity of structural SSNMR models, and they can also be readily applied to the analysis of protein–protein and protein–ligand interactions in challenging biomacromolecular systems including amyloid aggregates and membrane proteins. Additional studies are required to fully assess the utility of these PRE-based distance restraints for de novo protein structure refinement by solid-state NMR. These studies are currently in progress in our laboratory.

Acknowledgment. This work was supported by the National Science Foundation (CAREER Award MCB-0745754 to C.P.J.). We thank Dr. Angela M. Gronenborn for the GB1 plasmid, and Dr. Charles Schwieters for his assistance in generating the structural models of EDTA-M proteins.

Supporting Information Available: Tables with backbone amide ¹⁵N longitudinal PREs and ¹⁵N–Cu²⁺ distances for 28EDTA-Cu²⁺, and comparisons of experimental ¹⁵N longitudinal PREs and ¹⁵N–Cu²⁺ distances with the corresponding values obtained from structural models of 28EDTA-M and 53EDTA-M; figures with solution-state chemical shift differences between 53EDTA-Zn²⁺ and GB1, metal ion exchange kinetics in 53EDTA-M proteins, representative strips from 3D CONCA, NCACX, and NCOCX solid-state NMR spectra of 53EDTA-Zn²⁺, relative cross-peak intensities in 2D NCA solid-state NMR spectra of 53EDTA-Cu²⁺/Mn²⁺ and 53EDTA-Zn²⁺, 2D NCA spectra of 28EDTA-Cu²⁺ and representative measurements of residue-specific solid-state ¹⁵N R_1 rates in 28EDTA-Zn²⁺ and 28EDTA-Cu²⁺ (PDF). This material is available free of charge via the Internet at <http://pubs.acs.org>.

JA900224Z

Supporting Information

Paramagnetic Ions Enable Tuning of Nuclear Relaxation Rates and Provide Long-Range Structural Restraints in Solid-State NMR of Proteins

Philippe S. Nadaud, Jonathan J. Helmus, Stefanie L. Kall, and Christopher P. Jaroniec*

Department of Chemistry, The Ohio State University, Columbus, Ohio 43210
E-mail: jaroniec@chemistry.ohio-state.edu

Table S1. Backbone amide ^{15}N longitudinal PREs, Γ_1^{N} , and $^{15}\text{N}-\text{Cu}^{2+}$ distances, $r_{\text{N-Cu}}$, derived from R_1^{N} measurements in 28EDTA- Cu^{2+} and 28EDTA- Zn^{2+} .

| Residue | $R_1^{\text{N}}(\text{Cu}^{2+}) (\text{s}^{-1})$ | $R_1^{\text{N}}(\text{Zn}^{2+}) (\text{s}^{-1})$ | $\Gamma_1^{\text{N}} (\text{s}^{-1})^{\text{a}}$ | $r_{\text{N-Cu}} (\text{\AA})^{\text{b}}$ |
|---------|--|--|--|---|
| Q2 | 0.140 ± 0.012 | 0.100 ± 0.008 | 0.040 ± 0.014 | $17.8_{-0.9}^{+1.4}$ |
| L5 | 0.099 ± 0.002 | 0.053 ± 0.010 | 0.046 ± 0.010 | $17.4_{-0.6}^{+0.7}$ |
| I6 | 0.072 ± 0.004 | 0.047 ± 0.005 | 0.025 ± 0.006 | $19.2_{-0.7}^{+1.0}$ |
| G9 | 0.080 ± 0.002 | 0.074 ± 0.009 | 0.006 ± 0.009 | $24.4_{-3.5}^{+\infty}$ |
| T11 | 0.151 ± 0.004 | 0.140 ± 0.015 | 0.011 ± 0.016 | $22.1_{-3.0}^{+\infty}$ |
| K13 | 0.088 ± 0.003 | 0.067 ± 0.014 | 0.021 ± 0.014 | $19.8_{-1.6}^{+4.2}$ |
| G14 | 0.111 ± 0.003 | 0.091 ± 0.011 | 0.020 ± 0.011 | $20.0_{-1.4}^{+3.0}$ |
| T16 | 0.139 ± 0.005 | 0.094 ± 0.013 | 0.045 ± 0.014 | $17.4_{-0.8}^{+1.1}$ |
| V21 | 0.197 ± 0.005 | 0.128 ± 0.018 | 0.069 ± 0.019 | $16.2_{-0.6}^{+0.9}$ |
| T25 | 0.52 ± 0.11 | 0.055 ± 0.005 | 0.46 ± 0.11 | $11.8_{-0.4}^{+0.5}$ |
| E27 | 0.32 ± 0.04 | 0.043 ± 0.012 | 0.28 ± 0.04 | $12.9_{-0.3}^{+0.3}$ |
| C28 | 0.80 ± 0.18 | 0.045 ± 0.008 | 0.76 ± 0.18 | $10.9_{-0.4}^{+0.5}$ |
| V29 | 0.45 ± 0.03 | 0.023 ± 0.007 | 0.43 ± 0.04 | $12.0_{-0.2}^{+0.2}$ |
| G38 | 0.160 ± 0.010 | 0.072 ± 0.004 | 0.088 ± 0.011 | $15.6_{-0.3}^{+0.3}$ |
| D40 | 0.303 ± 0.007 | 0.174 ± 0.016 | 0.129 ± 0.017 | $14.6_{-0.3}^{+0.4}$ |
| G41 | 0.520 ± 0.021 | 0.432 ± 0.015 | 0.088 ± 0.026 | $15.6_{-0.7}^{+0.9}$ |
| E42 | 0.207 ± 0.009 | 0.104 ± 0.008 | 0.103 ± 0.012 | $15.2_{-0.3}^{+0.3}$ |
| W43 | 0.168 ± 0.004 | 0.059 ± 0.012 | 0.109 ± 0.013 | $15.1_{-0.3}^{+0.3}$ |
| T44 | 0.088 ± 0.006 | 0.050 ± 0.010 | 0.038 ± 0.012 | $17.9_{-0.8}^{+1.1}$ |
| T49 | 0.156 ± 0.011 | 0.126 ± 0.016 | 0.030 ± 0.019 | $18.7_{-1.5}^{+3.5}$ |
| T51 | 0.101 ± 0.008 | 0.064 ± 0.008 | 0.037 ± 0.011 | $18.0_{-0.8}^{+1.1}$ |
| F52 | 0.084 ± 0.004 | 0.038 ± 0.002 | 0.046 ± 0.004 | $17.4_{-0.3}^{+0.3}$ |
| T53 | 0.072 ± 0.004 | 0.036 ± 0.010 | 0.036 ± 0.011 | $18.1_{-0.8}^{+1.1}$ |
| T55 | 0.093 ± 0.003 | 0.043 ± 0.008 | 0.050 ± 0.009 | $17.1_{-0.4}^{+0.5}$ |
| E56 | 0.118 ± 0.002 | 0.074 ± 0.002 | 0.044 ± 0.003 | $17.5_{-0.2}^{+0.2}$ |

^a $\Gamma_1^{\text{N}} = R_1^{\text{N}}(\text{Cu}^{2+}) - R_1^{\text{N}}(\text{Zn}^{2+})$.

^bEstimated using Equation 1 of the main text with $g = 2.09$ and $T_{1e} = 2.5$ ns (c.f., Table 1).

Table S2. Comparison of experimental ^{15}N longitudinal PREs and $^{15}\text{N}-\text{Cu}^{2+}$ distances (c.f., Table 1) with corresponding values derived from a structural model of 53EDTA-M.

| Residue | Γ_1^{N} from Experiment (s^{-1}) | Γ_1^{N} from Structure (s^{-1}) | $r_{\text{N-Cu}}$ from Experiment (\AA) | $r_{\text{N-Cu}}$ from Structure (\AA) |
|---------|---|--|--|---|
| L5 | 0.146 ± 0.021 | 0.095 | $14.3^{+0.4}_{-0.3}$ | 15.5 |
| I6 | 0.179 ± 0.022 | 0.280 | $13.9^{+0.3}_{-0.3}$ | 12.9 |
| T11 | 0.125 ± 0.017 | 0.027 | $14.7^{+0.4}_{-0.3}$ | 19.0 |
| K13 | 0.107 ± 0.019 | 0.062 | $15.1^{+0.5}_{-0.4}$ | 16.6 |
| G14 | 0.157 ± 0.022 | 0.143 | $14.2^{+0.4}_{-0.3}$ | 14.5 |
| T18 | 0.029 ± 0.013 | 0.014 | $18.8^{+2.0}_{-1.1}$ | 21.2 |
| V21 | 0.018 ± 0.009 | 0.003 | $20.3^{+2.6}_{-1.4}$ | 27.1 |
| D22 | 0.029 ± 0.016 | 0.004 | $18.8^{+2.6}_{-1.3}$ | 25.8 |
| T25 | 0.021 ± 0.008 | 0.005 | $19.8^{+1.7}_{-1.0}$ | 25.0 |
| E27 | 0.030 ± 0.015 | 0.013 | $18.7^{+2.3}_{-1.2}$ | 21.6 |
| K28 | 0.010 ± 0.011 | 0.008 | $22.4^{+\infty}_{-2.7}$ | 23.4 |
| V29 | 0.010 ± 0.018 | 0.006 | $22.4^{+\infty}_{-3.6}$ | 24.3 |
| N37 | 0.007 ± 0.023 | 0.006 | $23.8^{+\infty}_{-5.2}$ | 24.5 |
| G38 | 0.016 ± 0.012 | 0.007 | $20.7^{+5.4}_{-1.9}$ | 24.1 |
| D40 | 0.040 ± 0.026 | 0.018 | $17.8^{+3.3}_{-1.4}$ | 20.5 |
| T44 | 0.17 ± 0.03 | 0.247 | $13.9^{+0.5}_{-0.4}$ | 13.2 |
| T49 | 0.19 ± 0.03 | 0.176 | $13.7^{+0.4}_{-0.3}$ | 14.0 |
| T51 | 0.18 ± 0.03 | 0.166 | $13.8^{+0.4}_{-0.4}$ | 14.1 |
| F52 | 0.271 ± 0.020 | 0.198 | $12.9^{+0.2}_{-0.2}$ | 13.7 |
| T55 | 0.26 ± 0.09 | 0.242 | $13.0^{+1.0}_{-0.6}$ | 13.2 |
| E56 | 0.20 ± 0.08 | 0.141 | $13.6^{+1.2}_{-0.7}$ | 14.5 |

Table S3. Comparison of experimental ^{15}N longitudinal PREs and $^{15}\text{N}-\text{Cu}^{2+}$ distances (c.f., Table S1) with corresponding values derived from a structural model of 28EDTA-M.

| Residue | Γ_1^{N} from Experiment (s^{-1}) | Γ_1^{N} from Structure (s^{-1}) | $r_{\text{N-Cu}}$ from Experiment (\AA) | $r_{\text{N-Cu}}$ from Structure (\AA) |
|---------|---|--|--|---|
| Q2 | 0.040 ± 0.014 | 0.009 | $17.8^{+1.4}_{-0.9}$ | 22.9 |
| L5 | 0.046 ± 0.010 | 0.011 | $17.4^{+0.7}_{-0.6}$ | 22.0 |
| I6 | 0.025 ± 0.006 | 0.009 | $19.2^{+1.0}_{-0.7}$ | 23.2 |
| G9 | 0.006 ± 0.009 | 0.005 | $24.4^{+\infty}_{-3.5}$ | 25.7 |
| T11 | 0.011 ± 0.016 | 0.003 | $22.1^{+\infty}_{-3.0}$ | 28.1 |
| K13 | 0.021 ± 0.014 | 0.003 | $19.8^{+4.2}_{-1.6}$ | 27.8 |
| G14 | 0.020 ± 0.011 | 0.003 | $20.0^{+3.0}_{-1.4}$ | 27.6 |
| T16 | 0.045 ± 0.014 | 0.006 | $17.4^{+1.1}_{-0.8}$ | 24.6 |
| V21 | 0.069 ± 0.019 | 0.057 | $16.2^{+0.9}_{-0.6}$ | 16.8 |
| T25 | 0.46 ± 0.11 | 0.464 | $11.8^{+0.5}_{-0.4}$ | 11.9 |
| E27 | 0.28 ± 0.04 | 0.235 | $12.9^{+0.3}_{-0.3}$ | 13.3 |
| C28 | 0.76 ± 0.18 | 0.764 | $10.9^{+0.5}_{-0.4}$ | 10.9 |
| V29 | 0.43 ± 0.04 | 0.422 | $12.0^{+0.2}_{-0.2}$ | 12.1 |
| G38 | 0.088 ± 0.011 | 0.016 | $15.6^{+0.3}_{-0.3}$ | 20.7 |
| D40 | 0.129 ± 0.017 | 0.022 | $14.6^{+0.4}_{-0.3}$ | 19.7 |
| G41 | 0.088 ± 0.026 | 0.027 | $15.6^{+0.9}_{-0.7}$ | 19.0 |
| E42 | 0.103 ± 0.012 | 0.020 | $15.2^{+0.3}_{-0.3}$ | 20.1 |
| W43 | 0.109 ± 0.013 | 0.030 | $15.1^{+0.3}_{-0.3}$ | 18.8 |
| T44 | 0.038 ± 0.012 | 0.023 | $17.9^{+1.1}_{-0.8}$ | 19.6 |
| T49 | 0.030 ± 0.019 | 0.004 | $18.7^{+3.5}_{-1.5}$ | 26.0 |
| T51 | 0.037 ± 0.011 | 0.010 | $18.0^{+1.1}_{-0.8}$ | 22.7 |
| F52 | 0.046 ± 0.004 | 0.016 | $17.4^{+0.3}_{-0.3}$ | 20.9 |
| T53 | 0.036 ± 0.011 | 0.016 | $18.1^{+1.1}_{-0.8}$ | 20.9 |
| T55 | 0.050 ± 0.009 | 0.011 | $17.1^{+0.5}_{-0.4}$ | 22.2 |
| E56 | 0.044 ± 0.003 | 0.007 | $17.5^{+0.2}_{-0.2}$ | 24.1 |

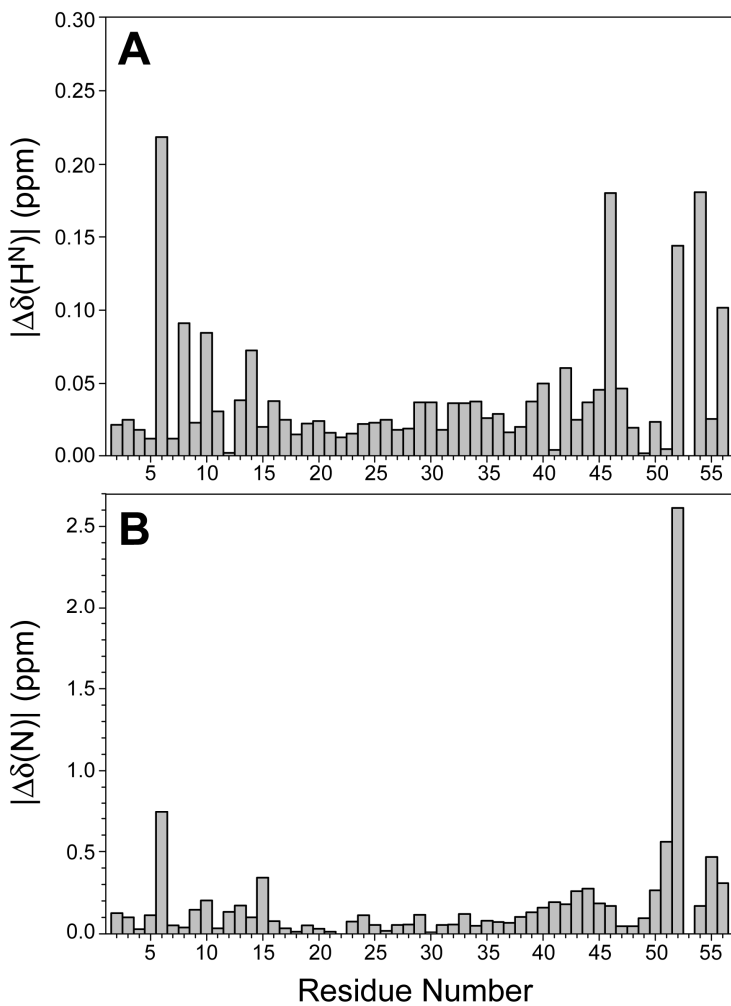


Figure S1. Absolute chemical shift differences in solution for amide ^1H (A) and ^{15}N (B) nuclei in 53EDTA-Zn $^{2+}$ and wild-type GB1 as a function of residue number. The average $^1\text{H}^N$ and ^{15}N absolute chemical shift differences were $\langle|\Delta\delta(\text{H}^N)|\rangle = 0.04 \pm 0.05$ ppm and $\langle|\Delta\delta(\text{N})|\rangle = 0.2 \pm 0.4$ ppm, respectively. Shift differences involving the mutation site (residue 53) were excluded from the plots and calculated averages.

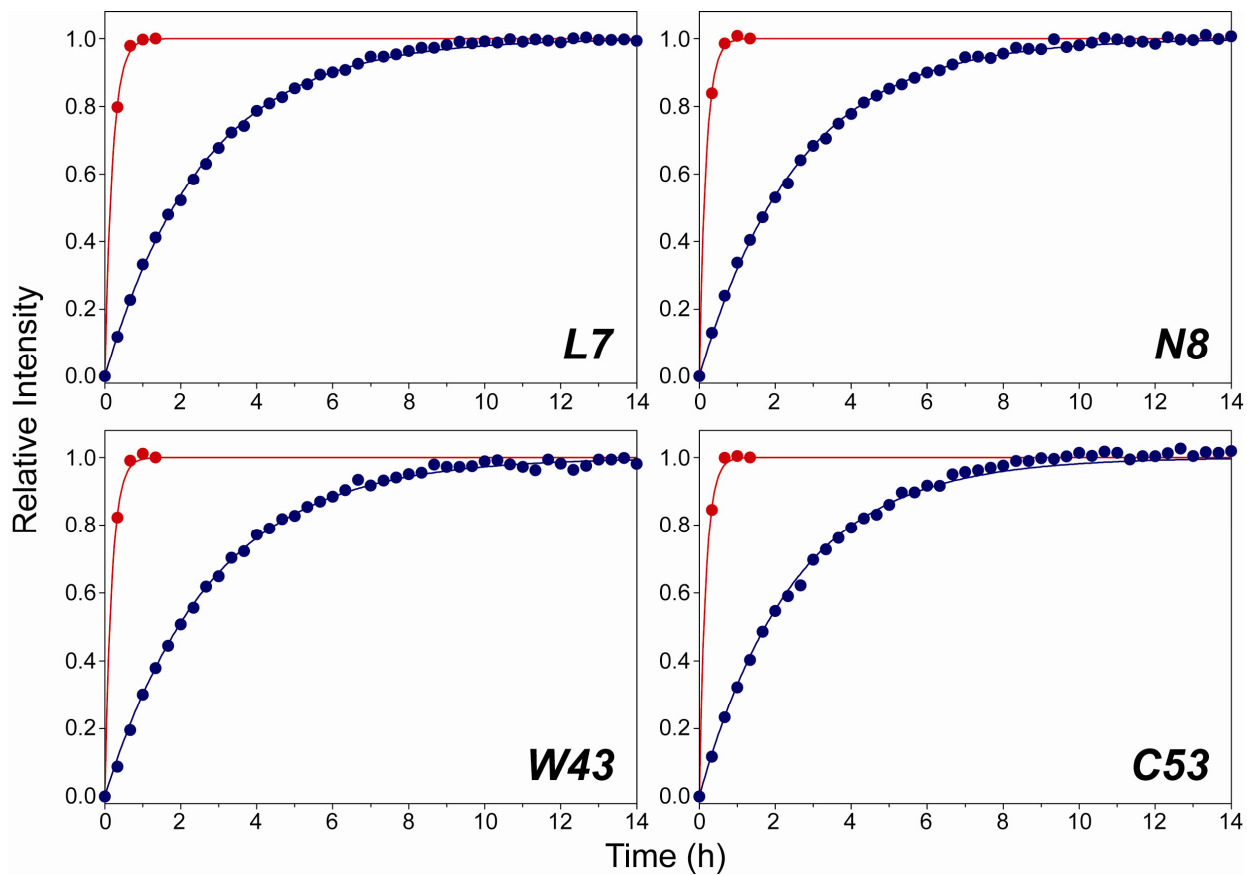


Figure S2. Metal ion exchange kinetics monitored via the appearance in 2D ^1H - ^{15}N HSQC spectra (c.f., Figure 3 of the main text) of cross-peaks characteristic of ^{15}N -53EDTA- Zn^{2+} following the addition of a 3-fold molar excess of na-53EDTA- Zn^{2+} to ^{15}N -labeled 53EDTA- Mn^{2+} (red circles) and 53EDTA- Cu^{2+} (blue circles). Trajectories for four representative residues in the vicinity of the metal binding site (L7, N8, W43 and C53) are shown. The relative cross-peak intensity as a function of time is given by $[I(t) - I_0]/[I_f - I_0]$, where $I(t)$, I_0 , I_f are the instantaneous, initial and final peak intensities, respectively. Also shown are the best-fits to rising single exponentials.

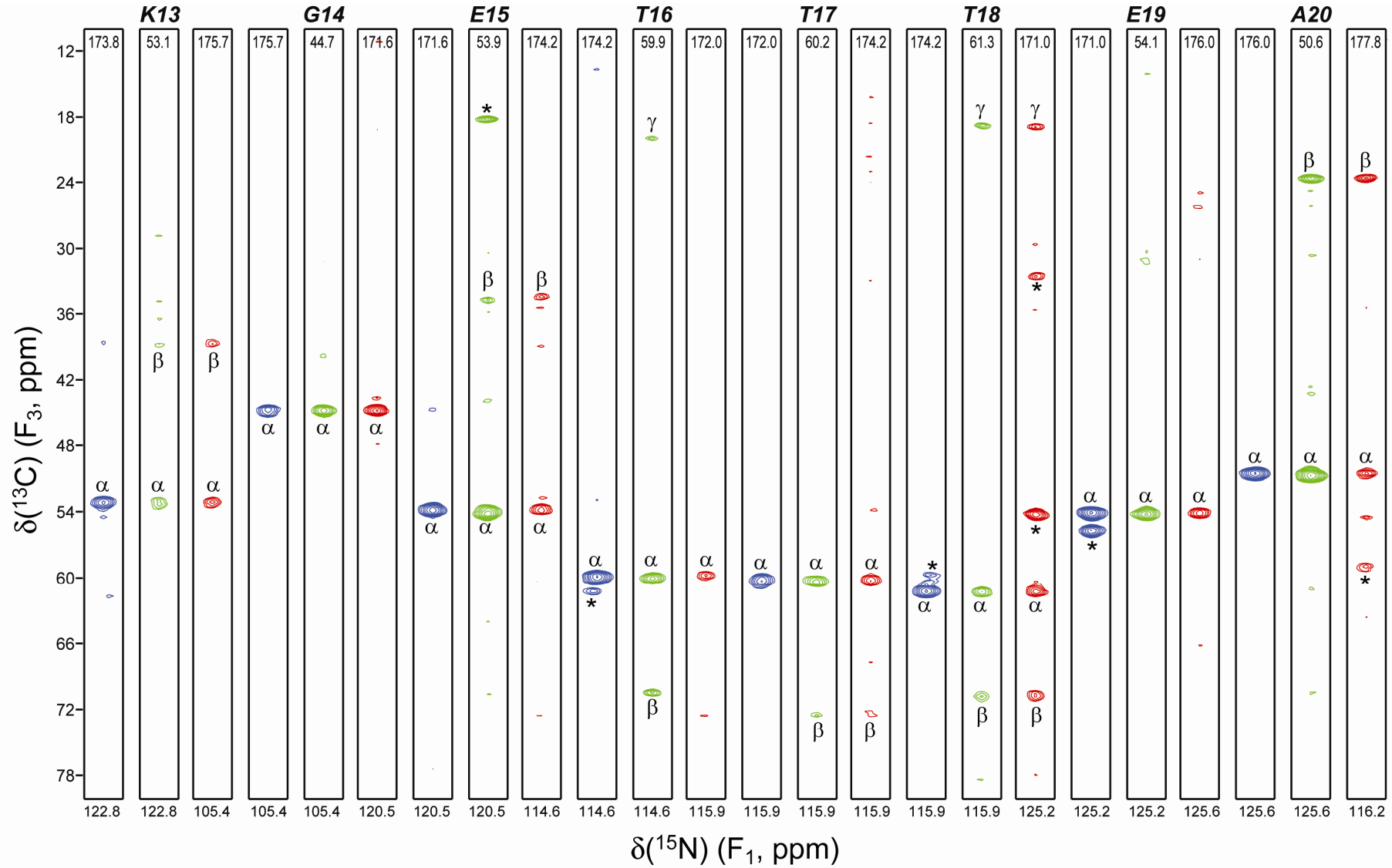


Figure S3. Representative $[F_1(^{15}\text{N}), F_3(^{13}\text{C})]$ -strips for residues K13-A20 from 3D CONCA (blue contours), NCACX (green contours) and NCOCX (red contours) spectra of 53EDTA-Zn²⁺ recorded at 500 MHz ^1H frequency and 11.111 kHz MAS rate. The $F_1(^{15}\text{N})$ and $F_2(^{13}\text{C})$ frequencies are listed below and inside each strip, respectively. Major cross-peaks corresponding to α , β and γ ^{13}C resonances in F_3 are indicated, and minor peaks from neighboring spectral planes are marked by asterisks. The key data acquisition and processing parameters were analogous to those used in our previous studies of this type.^{1,2}

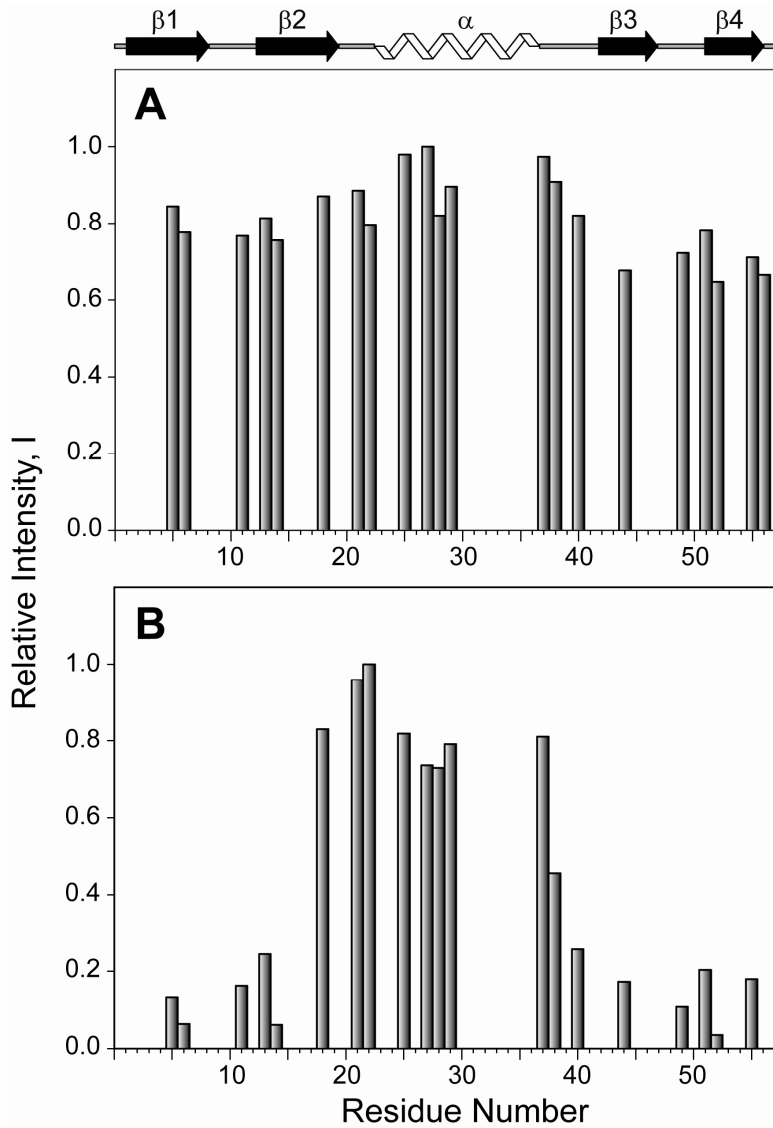


Figure S4. Cross-peak intensities (heights), I , in 2D ^{15}N - $^{13}\text{C}\alpha$ SSNMR correlation spectra (c.f., Figure 5) of (A) 53EDTA- Cu^{2+} and (B) 53EDTA- Mn^{2+} relative to 53EDTA- Zn^{2+} as a function of residue number. The intensities were normalized according to $I = (I_{\text{param}}/I_{\text{diam}})/(I_{\text{param}}/I_{\text{diam}})_{\text{max}}$, where I_{param} and I_{diam} are the peak heights in 53EDTA- $\text{Cu}^{2+}/\text{Mn}^{2+}$ and 53EDTA- Zn^{2+} spectra, respectively, and $(I_{\text{param}}/I_{\text{diam}})_{\text{max}}$ is the maximum $(I_{\text{param}}/I_{\text{diam}})$ value for each pair of spectra. Peak heights were extracted using the program Sparky (Goddard, T. D.; Kneller, D. G., SPARKY 3, University of California, San Francisco); for peaks with severely reduced intensity in the 53EDTA- Mn^{2+} spectrum, the intensity at the exact peak position in the 53EDTA- Zn^{2+} spectrum was used, and for peaks where no quantitative measurement could be made due to overlap, the value of I was set to zero.

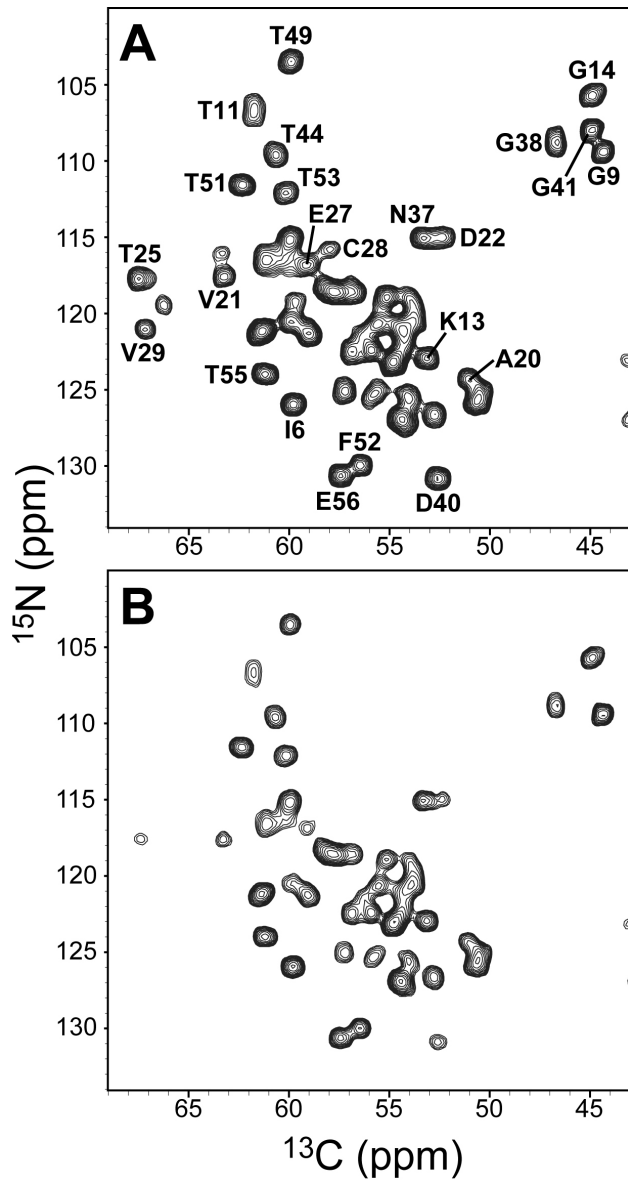


Figure S5. 2D NCA spectra of 28EDTA- Cu^{2+} recorded using the pulse scheme shown in Figure 7A of the main text with (A) $\tau = 0$ s and (B) $\tau = 4$ s. Selected resonance assignments are indicated (complete backbone assignments were established using a set of 3D spectra analogous to those shown in Figure S3).

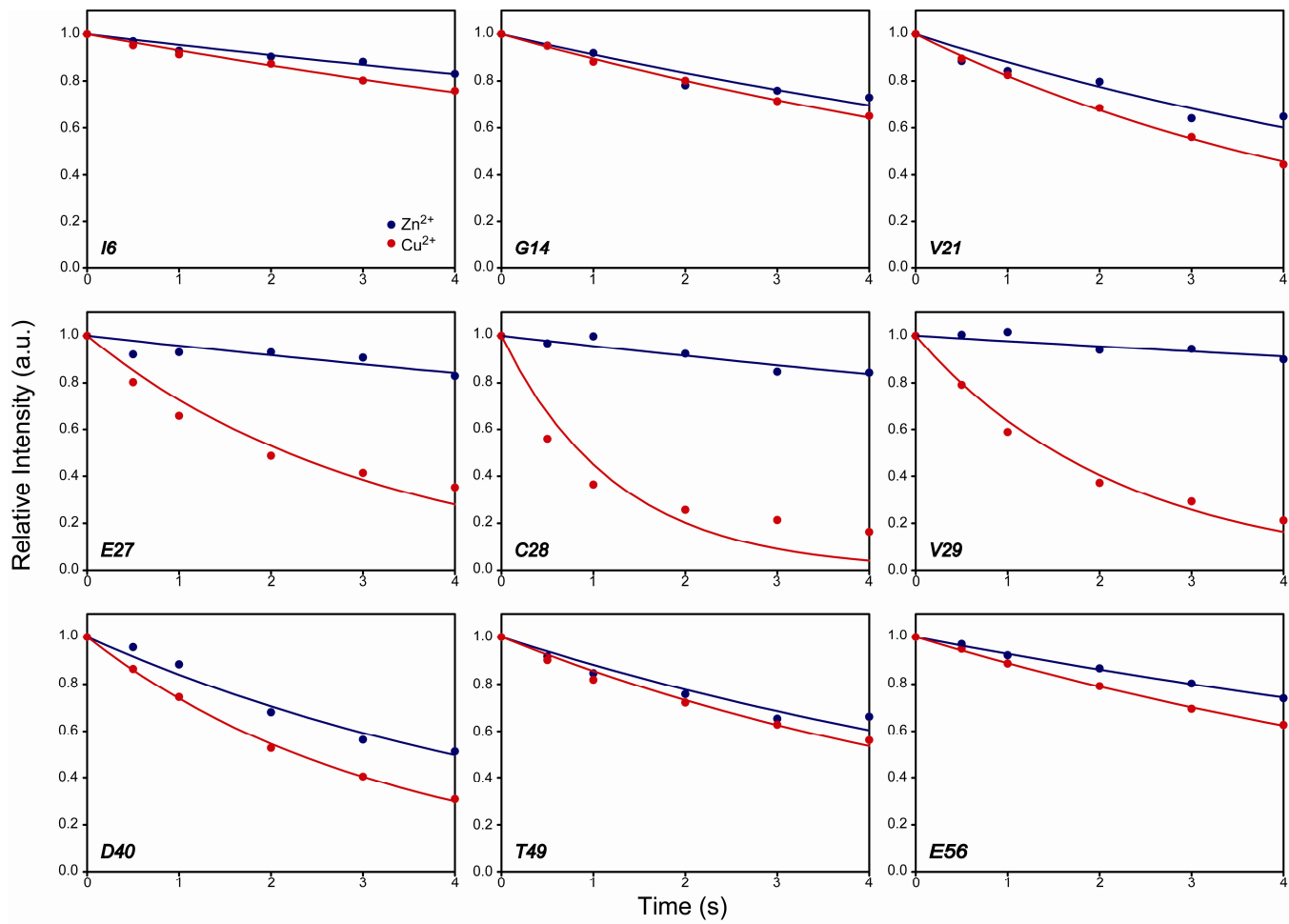


Figure S6. Representative measurements of residue-specific solid-state ^{15}N R_1 rates in 28EDTA-Zn²⁺ (blue circles) and 28EDTA-Cu²⁺ (red circles) obtained using the pulse scheme in Figure 7A of the main text. Best-fits to decaying single exponentials are shown as solid lines. See Table S1 for a summary of the fitting results.

References

- (1) Nadaud, P. S.; Helmus, J. J.; Jaroniec, C. P. *Biomol. NMR Assign.* **2007**, 1, 117-120.
- (2) Helmus, J. J.; Surewicz, K.; Nadaud, P. S.; Surewicz, W. K.; Jaroniec, C. P. *Proc. Natl. Acad. Sci. USA* **2008**, 105, 6284-6289.